Marine Environmental Research 212 (2025) 107515

Contents lists available at ScienceDirect

Marine Environmental Research

journal homepage: www.elsevier.com/locate/marenvrev

Massive carbon inputs from fish farming reduce carbon sequestration capacity in a macroalgae mariculture area

Wei Yang [a], Yingxu Wu [a,b,*], Yanmei Liu [a], Peiqiang Zhuang [a], Chenglong Li [a], Jianhang Zhang [a], Yingfeng Chen [a], Yanpei Zhuang [a], Hongyang Lin [c], Huaji Qiu [b], Youjun Huang [d], Weijie Qiu [e], Wei-Jun Cai [f], Liqi Chen [a], Di Qi [a,**]

[a] Polar and Marine Research Institute, College of Harbor and Coastal Engineering, Jimei University, Xiamen, 361000, PR China
[b] Xiamen Lantan Space Technology Company, Xiamen, 361023, PR China
[c] State Key Laboratory of Marine Environmental Science, College of Ocean and Earth Sciences, Xiamen University, Xiamen, 361102, PR China
[d] Xiamen Identity Treasure Network Technology Company, Xiamen, 361009, PR China
[e] Fujian Yida Food Co., Ltd, Lianjiang, 350500, PR China
[f] School of Marine Science and Policy, University of Delaware, Newark, DE, United States

ARTICLE INFO

Keywords:
Macroalgae mariculture
Marine carbon dioxide removal
CO_2 source and sink status
Carbonate system dynamics
DIC stable carbon isotope

ABSTRACT

Macroalgae mariculture is promoted as a marine carbon dioxide removal (mCDR) strategy, particularly in East Asia. In practice, however, macroalgae is frequently co-cultured with fish and shellfish, complicating carbon budgets and potentially altering net carbon metabolism. While most work has emphasized organic carbon cycles, carbonate system responses under integrated aquaculture remain underexplored. In this study, we conducted seasonal surveys in Sansha Bay, one of the world' largest mariculture zones. Contrary to expectation, the bay persistently outgassed CO_2 during winter (the seaweed growth peak season), spring, and fall. Sea surface CO_2 partial pressure (pCO_2) reached 500–1100 μatm with air-sea CO_2 fluxes of 2.1–7.0 mmol m^{-2} d^{-1}. Against an estimated natural background of 200 μatm (a strong sink), long-term effects of cultivation diverged by trophic group: seaweed cultivation lowered pCO_2 by 42 ± 5 μatm, shellfish farming increased it by 36 ± 4 μatm, and fish farming raised it by 375 ± 18 μatm, elevating mean pCO_2 to ~567 ± 20 μatm and transforming the system from a CO_2 sink to a source. In this semi-enclosed bay, dissolved inorganic carbon (DIC) generated from fish farming overwhelms algal uptake, driving increases in DIC and pCO_2 and reducing the region's carbon sequestration capacity. Seasonal submarine groundwater discharge added ~30–60 μatm to pCO_2, and short-term mariculture activities could episodically elevate pCO_2 up to 1100 μatm. Analysis of the dissolved inorganic carbon stable carbon isotope ($\delta^{13}C_{DIC}$) indicates that seasonal increases in DIC and pCO_2 in Sansha Bay are due to the decomposition of residual seaweed biomass in late spring and organic matter respiration from fish feed in fall. To achieve mCDR and protect coastal environments, it is essential to reduce formulated feed use or develop alternative environmentally friendly fish farming methods.

1. Introduction

The rising levels of atmospheric CO_2 and their harmful environmental impacts are well acknowledged (Friedlingstein et al., 2022; Mathis et al., 2024). With varying outcomes for human society and oceans under different anthropogenic CO_2 emission scenarios, there is an urgent need to reduce emissions and develop negative emission technologies (Cai and Jiao, 2022; Froehlich et al., 2019; Gao et al., 2022a, 2022b; Li et al., 2022). Among marine CO_2 removal (mCDR) strategies, macroalgae cultivation, nutrient fertilization, artificial upwelling/downwelling, and ocean alkalinity enhancement show promise for achieving carbon neutrality and mitigating climate change effects (Cai and Jiao, 2022; Jiao et al., 2018, 2021; Wang et al., 2021). Driven by policy incentives, macroalgae mariculture has expanded

This article is part of a special issue entitled: EBERCA published in Marine Environmental Research.

* Corresponding author. Polar and Marine Research Institute, College of Harbor and Coastal Engineering, Jimei University, Xiamen, 361000, PR China.
** Corresponding author.
E-mail addresses: yingxu.wu@jmu.edu.cn (Y. Wu), qidi@jmu.edu.cn (D. Qi).

https://doi.org/10.1016/j.marenvres.2025.107515
Received 25 April 2025; Received in revised form 13 August 2025; Accepted 1 September 2025
Available online 6 September 2025

significantly in East Asian countries like China since the 1990s. This growth has led to substantial annual harvests for food, bioenergy, and other applications (Guan et al., 2022; Tang et al., 2018; Weitzman et al., 2019; Xie et al., 2022).

Macroalgae mariculture areas are known for high productivity and carbon sequestration capacity, making them vital contributors to blue carbon in coastal zones (Clawson et al., 2022; Froehlich et al., 2019; Troell et al., 2022; Wang et al., 2021; Zhang et al., 2017). In these regions, air-sea CO_2 fluxes at the sea surface are mainly influenced by the gradient of CO_2 partial pressure (pCO_2) between surface seawater and the atmosphere. The former is regulated by biological processes such as photosynthesis and respiration (Yang et al., 2022). For example, during seaweed growth, photosynthesis consumes dissolved inorganic carbon (DIC), reducing seawater pCO_2. Conversely, respiration of organic matter (e.g., residual seaweed biomass) increases DIC levels while raising pCO_2. These processes drive seasonal cycles of sea surface pCO_2 in macroalgae mariculture areas (Ji et al., 2021; Lin et al., 2019; Wei et al., 2016; Xie et al., 2022).

Globally, 7.2×10^7 km^2 of ocean is environmentally suitable for farming various species (Oyinlola et al., 2018). Macroalgae are typically cultivated alongside mixed fish and shellfish farming, a common practice in many aquaculture regions. In China, integrated aquaculture has demonstrated both environmental and economic benefits, accounting for 40 % of the country's mariculture production (Fang et al., 2020; Liu et al., 2022; Qiu et al., 2013; Xie et al., 2022). While macroalgae growth absorbs DIC, making these areas strong CO_2 sinks, intensified mariculture activities, such as the use of formulated feed, can led to increased DIC levels in bay waters and elevate seawater pCO_2 through decomposition (Ji et al., 2021; Wei et al., 2016). Most studies on mariculture have focused on the organic carbon cycles with limited exploration of carbonate parameters related to integrated practices. The dynamics of pCO_2 and CO_2 sources/sinks in integrated mariculture area are influenced by complex physical, biochemical, and anthropogenic processes that require further investigation.

Sansha Bay, one of the largest global mariculture zones, produces significant amounts of seaweed (*Saccharina japonica* and *Gracilaria lemaneiformis*), fish (*Pseudosciaena crocea*), and shellfish (*Haliotis discus hannai*), with annual outputs of 296 kt, 327 kt, and 259 kt respectively in 2021. Recent studies emphasize Sansha Bay's potential as a carbon sink due to macroalgae mariculture converting inorganic carbon into particulate organic carbon (Han et al., 2024; Wang et al., 2023a, 2023b). This process is expected to reduce DIC levels while maintaining a strong CO_2 sink at the sea surface. However, during our observation in the main channel of Sansha Bay and the secondary inner bay Dongwuyang, we

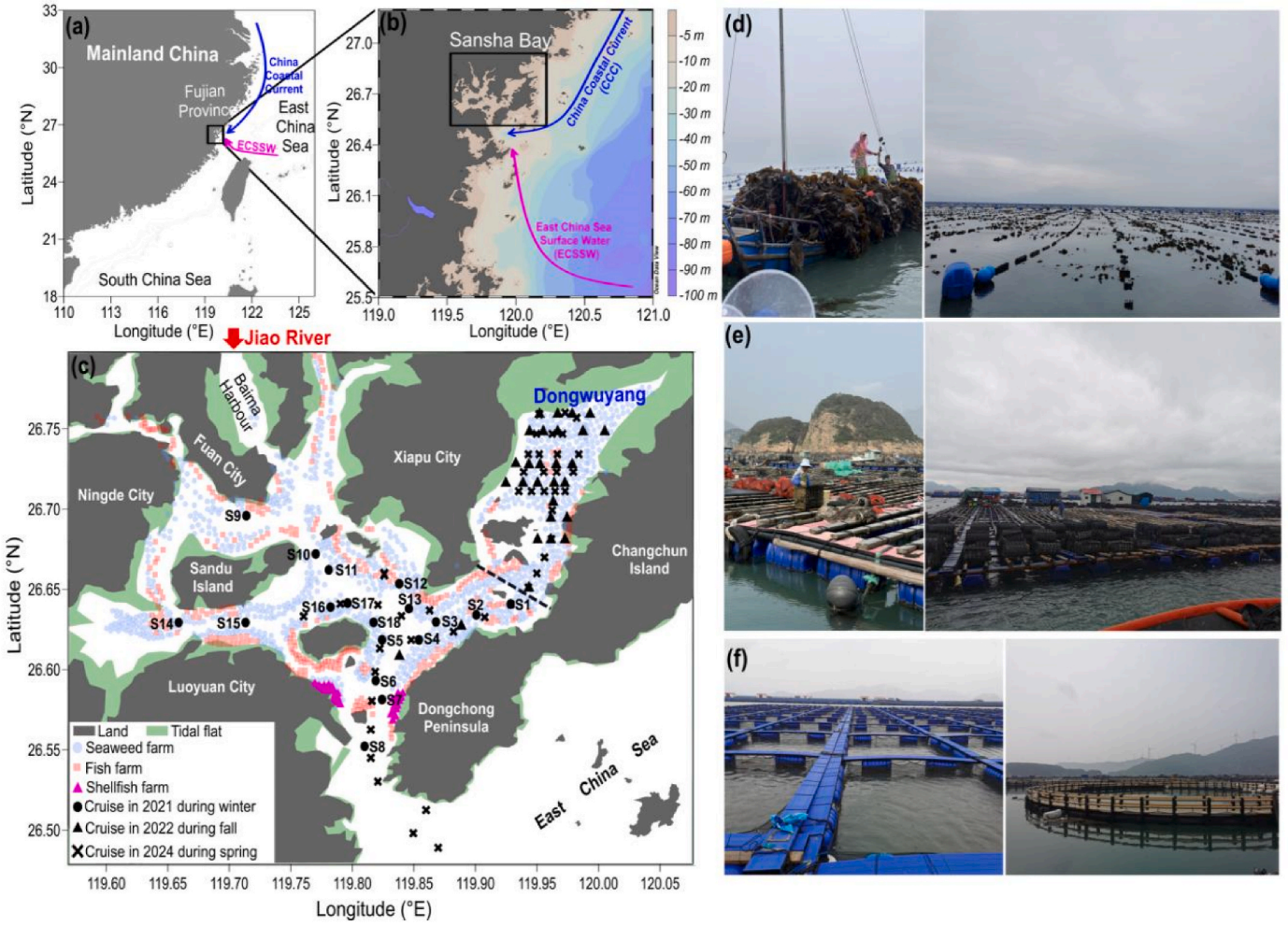

Fig. 1. Maps showing the sampling area in Fujian Province (a), coastal currents that influence Sansha Bay (b), locations of sampling stations during the winter cruise in 2021 (black circles), fall cruise in 2022 (black triangles), and spring cruise in 2024 (black crosses) (c), and the facilities for seaweed cultivation (d), shellfish farming (e), and fish farming (f). In panels (a) and (b), blue and pink arrows represent schematic depictions of circulation features within Sansha Bay, including the China Coastal Current (CCC) in cold seasons and the East China Sea Surface Water (ECSSW) in warm seasons. In panel (c), blue, orange, and pick markers denote regions predominantly occupied by seaweed farms, fish farms, and shellfish farms, respectively. (For interpretation of the references to colour in this figure legend, the reader is referred to the Web version of this article.)

detected significant CO_2 outgassing events in winter, spring, and fall. Sea surface pCO_2 levels exceeded atmospheric levels by 200–550 μatm. This contradicts the anticipated CO_2 sink nature of macroalgae mariculture. Therefore, this study aims to identify the causes of these CO_2 sources and quantify various processes regulating DIC and pCO_2 dynamics.

2. Material and methods

2.1. Study area

Sansha Bay (26°30′-26°58′E, 119°26′-120°10′N) is a semi-enclosed bay in northeastern Fujian Province (Fig. 1a), covering an area of ~675 km^2 (Ji et al., 2021; Lin et al., 2019; Xie et al., 2022). It is bordered by Ningde, Xiapu, and Luoyuan and features secondary bays like Baima Harbour, Yantian Harbour, and Dongwuyang (Fig. 1b and c). A narrow passage about 3 km wide connects the inner nearshore waters to the outer East China Sea (ECS). Within Sansha Bay, seaweed rafts coexist with fish cages throughout the area, while floating shellfish cages are primarily found at the bay's mouth (Fig. 1c). Seaweed cultivation occurs from November to May. In contrast, shellfish and fish are grown and harvested year-round (Ji et al., 2021; Xie et al., 2022).

The hydrological characteristics of Sansha Bay are significantly influenced by the China Coastal Current (CCC) in cold seasons and the East China Sea Surface Water (ECSSW) in warm seasons (Fig. 1a and b) (Han et al., 2013, 2021a, 2024). In late fall and winter, the CCC flows southward along the Chinese mainland from the ECS or further north, bringing cold, fresh, nutrient-rich waters that impact Sansha Bay's biogeochemistry (Han et al., 2013, 2021; Yang et al., 2021a). During summer and early fall, driven by the southwest monsoon, ECSSW enters through Dongchong Channel, resulting in higher seawater temperatures than in winter (Han et al., 2021a; Ji et al., 2021; Lin et al., 2019). Additionally, freshwater discharge from Jiao River, the largest river nearby, significantly affects Sansha Bay's hydrographic characteristics (Fig. 1c) (Han et al., 2021a).

Submarine groundwater discharge (SGD), which is water flow from seafloor to coastal ocean at permeable sediment-water interfaces, plays a prominent role here (Dai et al., 2021; Wang et al., 2014; Yang et al., 2022). SGD is characterized by higher concentrations of nutrients and inorganic carbon compared to offshore surface waters. This impacts blue carbon budgets as well as coastal eutrophication, acidification, hypoxia, and pollution levels (Jiang et al., 2021; La Valle et al., 2023; Liu et al., 2023; Nguyen, 2024). In Sansha Bay specifically, SGD influences have been observed through radium isotopes activity measurements (^{224}Ra and ^{228}Ra), quantifying its effects alongside associated nutrient and carbon fluxes (Wang et al., 2014, 2018).

Throughout all seasons, a water mass with lower salinity than ECSSW and CCC was observed in Sansha Bay (referred to as Sansha Bay Water, SBW) (Han et al., 2021a). It originated from a mix of freshwater from coastal river (like Jiao River) and offshore ECSSW and/or CCC (Fig. 1b and c). Intensive mariculture activities, such as seaweed cultivation, shellfish and fish farming (Fig. 1d–f), have also influenced its composition (Han et al., 2021a, 2024). With nutrient input from these activities, SBW has much higher nutrient concentrations compared to other water masses (Bu et al., 2024; Han et al., 2021a; Wang et al., 2024).

2.2. Sampling and analyses

Sampling was conducted onboard the Min-Ning-YU-YUN-F620 and F580 in 2021 (December 11–12, winter), 2022 (November 17–19, fall), and 2024 (April 4–7, spring) (Fig. 1c). Observations and water samples were collected primarily in Dongwuyang during the fall cruise and in the main channel during winter. The spring cruise covered both sub-regions. Temperature, salinity, and depth at each station were measured with a Seabird® WQM 2019 CTD sensor during fall and winter cruises; in spring, an RBR CTD sensor was used for these measurements.

Water samples were collected at various depths using a 5L Niskin bottle during the cruise. To reduce uncertainties from atmospheric CO_2, DIC and TA samples were taken with Tygon® bubble-free tubing to ensure sample overflow. At sampling, 0.2 ml of saturated $HgCl_2$ solution was added to both DIC and TA samples, which were then stored in darkness before being analyzed within 1 month at a land-based laboratory. DIC was measured by acidifying a 0.5 mL water sample and quantifying CO_2 with a Li-Cor 7000 non-dispersive infrared (NDIR) spectrometer (AS-C2, Apollo SciTech Inc., USA), achieving an accuracy better than ±0.1 % (Cai et al., 2004). TA was determined via potentiometric Gran titration (AS-ALK1+, Apollo SciTech Inc., USA) with an accuracy of ±2.0 μmol kg^{-1} (Cai et al., 2004). The accuracy of DIC and TA measurements was confirmed through calibration against certified reference materials from A. G. Dickson, Scripps Institution of Oceanography, U.S.A., ensuring an accuracy better than ±2.0 μmol kg^{-1}.

During the 2022 and 2024 cruises, sea surface temperature (SST), sea surface salinity (SSS), and pCO_2 were measured using an underway pumping system. Given the mixed layer depth of ~4–8 m across all seasons (Bu et al., 2024; Han et al., 2021a, 2024), surface water was continuously pumped from a side intake at ~2–3 m depth. Temperature and conductivity were recorded continuously with an Idronaut Multiparameter "Flow Through" CTD recorder. A continuous-flow underway system with a cylinder-type equilibrator filled with plastic balls was used for air-sea equilibration (Zhai et al., 2005). The CO_2 mole fraction in dry air (xCO_2) was measured continuously using a Li-Cor® 7000 NDIR detector, calibrated against CO_2 gas standards every 4 h (e.g., concentrations of 204, 402, 591, and 994 μmol mol^{-1}). The accuracy of xCO_2 measurements and pCO_2 data processing was <1 % (Zhai et al., 2005, 2013). Air pCO_2 was determined every half hour; the bow intake for atmospheric air collection was positioned ~5 m above the water surface to prevent ship contamination.

As there were no in situ measurements of surface pCO_2 during the winter cruise in 2021, we calculated them from DIC and TA. These values were used in subsequent discussions. The effects of various processes on pCO_2 dynamics were assessed using the CO2SYS program (version 1.1) based on measured DIC and TA (van Heuven et al., 2011). Dissociation constants for carbonic acid and bisulfate came from Dickson (1990) and Lueker et al. (2000), respectively, while the total borate salinity relationship was derived from Lee et al. (2010). For December, the average background atmospheric CO_2 concentration (xCO_2) was obtained from Mauna Loa Observatory in Hawaii (https://scrippsco2.ucsd.edu/data/atmospheric_co2/primary_mlo_co2_record.html). Sea level pressure and wind speed data were sourced from the fifth generation ECMWF atmospheric reanalysis (ERA5; https://www.ecmwf.int/en/forecasts/dataset/ecmwf-reanalysis-v5).

2.3. Analyses of DO, AOU, and $\delta^{13}C_{DIC}$

During the spring cruise in 2024 and fall cruise in 2022, dissolved oxygen (DO) samples were collected, fixed and titrated on board using the Winkler procedure with an uncertainty of <0.5 %. Apparent oxygen utilization (AOU) was calculated by subtracting field-measured DO from air-equilibrated DO, which was determined based on temperature, salinity, and local air pressure following Benson and Krause (1984). A positive AOU indicates net community respiration while a negative value suggests net community production (Chen et al., 2022).

The determination of DIC stable carbon isotopes ($\delta^{13}C_{DIC}$) followed DIC analysis. Pure CO_2 gas was extracted from a 3 mL DIC sample by adding phosphoric acid to seawater samples. The gaseous CO_2 was dried and analyzed using a cavity ring-down spectroscopy analyzer (model: Picarro G2131-i) for $\delta^{13}C_{DIC}$ measurement, achieving precision better than 0.1 ‰. Further details on the determination and calculation processes can be found in Chen et al. (2022) and Zhao et al. (2020).

2.4. Air-sea CO_2 flux estimation

We quantified the net air-sea CO_2 fluxes, F (mmol m^{-2} d^{-1}), between surface water and the atmosphere following Takahashi et al. (2009):

$$F = k \times a \times \Delta pCO_2 \quad (1)$$

where k is the gas transfer velocity (m d^{-1}), a is the solubility of CO_2 (mol kg^{-1} atm^{-1}; Weiss, 1974), and ΔpCO_2 is the pCO_2 difference between surface water and atmosphere (μatm). A positive F indicates net CO_2 outgassing from sea to atmosphere, while a negative F indicates net CO_2 sinking from atmosphere to sea. The gas transfer velocity k related to wind speed was parameterized using the empirical function of Wanninkhof (2014):

$$k = 0.251 \times U_{10}^2 \times (S_c/660)^{-0.5} \quad (2)$$

where U_{10} is wind speed. In our calculations, U_{10} values were recorded as follows: 3.0 ± 0.2 m s^{-1} during winter 2021; 2.6 ± 2.5 m s^{-1} in the main channel and 3.6 ± 2.5 m s^{-1} in Dongwuyang during spring 2024; and finally, 2.4 ± 1.1 m s^{-1} in Dongwuyang for fall 2022. *Sc* is the Schmidt number for CO_2, calculated using the equations of Wanninkhof (2014).

2.5. Quantification and apportionment of the dynamics of DIC and TA resulting from different mariculture activities

In coastal ecosystems, the dynamics of DIC and TA are influenced by various processes, which can be quantified using a two end-member mixing model (Yang et al., 2022). In this model, salinity serves as a conservative tracer:

$$F_1+F_2 = 1 \quad (3)$$

$$S_1 \times F_1+S_2 \times F_2=S_X \quad (4)$$

S_x is the salinity of seawater samples; S_1 and S_2 are the salinities of different end members; F_1 and F_2 represent their respective fractional contributions. The concentrations of DIC and TA from the conservative mixing (DIC^{cons} and TA^{cons}) can be predicted as follows:

$$DIC^{cons} = DIC_1 \times F_1+DIC_2 \times F_2 \quad (5)$$

$$TA^{cons} = TA_1 \times F_1+TA_2 \times F_2 \quad (6)$$

DIC_1 and DIC_2, along with TA_1 and TA_2, denote the values for different end members. The difference between measured values (DIC^{meas} and TA^{meas}) and conservative estimates (DIC^{cons} and TA^{cons}), referred to as ΔDIC and ΔTA, indicate non-conservative additions/removals from other sources/processes:

$$\Delta DIC = DIC^{meas}\text{-}DIC^{cons} \quad (7)$$

$$\Delta TA = TA^{meas}\text{-}TA^{cons} \quad (8)$$

In Sansha Bay, changes in DIC and TA are likely driven by seaweed cultivation, shellfish farming, fish farming, and net $CaCO_3$ dissolution/precipitation. We attributed these changes to specific processes as follows:

$$\Delta DIC = \Delta DIC_{Seaweed}+\Delta DIC_{Shellfish}+\Delta DIC_{Fish}+\Delta DIC_{CaCO3} \quad (9)$$

$$\Delta TA = \Delta TA_{Seaweed}+\Delta TA_{Shellfish}+\Delta TA_{Fish}+\Delta TA_{CaCO3} \quad (10)$$

where each term represents changes in DIC or TA due to associated activities.

In a semi-enclosed bay, most carbon from mariculture is exported to the adjacent marginal sea through water exchange (Han et al., 2024). However, some carbon (as DIC) accumulates in the bay. Assuming that the mariculture structure in Sansha Bay has remained stable over decades, an input of 1×10^4 tons C from these activities increases seawater DIC by α μmol kg^{-1}. Thus, equations (9) and (10) could be rewritten as:

$$\Delta DIC = (-C_{net\text{-}seaweed} + C_{net\text{-}shellfish} + C_{net\text{-}fish}) \times \alpha+\beta \quad (11)$$

$$\Delta TA=(-C_{net\text{-}seaweed} + C_{shellfish\ respiration} + C_{net\text{-}fish}) \times \alpha \times (-17/106)\text{-}C_{shellfish\text{-}shells} \times \alpha \times 2+\beta \times 2 \quad (12)$$

$$C_{net\text{-}shellfish} = C_{shellfish\ respiration}\text{-}C_{shellfish\text{-}shells} \quad (13)$$

where $C_{net\text{-}seaweed}$ and $C_{net\text{-}fish}$ represent net DIC removal and input from seaweed cultivation and fish farming, respectively. The term $C_{net\text{-}shellfish}$ indicates net DIC removal related to shellfish farming, which includes organic matter respiration ($C_{shellfish\ respiration}$) and consumption during shell formation ($C_{shellfish\text{-}shells}$). The coefficient −17/106 reflects changes in TA due to biological DIC generation based on the Redfield Ratio (Dong et al., 2017; Redfield et al., 1963). β and 2β account for increases in both DIC and TA from natural $CaCO_3$ dissolution (Dong et al., 2017; Salt et al., 2016; Salter et al., 2014).

2.6. Tracing the origin of the oxygen-consuming organic matter (OM) using $\delta^{13}C_{DIC}$

The fractions of F_1 and F_2 were used to predict conservative concentrations of $\delta^{13}C_{DIC}$ from mixing, as follows:

$$(\delta^{13}C_{DIC}^{cons} \times DIC^{cons}) = \delta^{13}C_1 \times DIC_1 \times F_1+\delta^{13}C_2 \times DIC_2 \times F_2 \quad (14)$$

where $\delta^{13}C_1$ and $\delta^{13}C_2$ represent the DIC stable carbon isotope compositions of different end members.

In seawater, the composition of $\delta^{13}C_{DIC}$ is fractionated with changes in DIC concentrations, which helps identify processes regulating DIC dynamics (Chen et al., 2022; Su et al., 2017; Wang et al., 2016; Zhang et al., 2025; Zhao et al., 2020). By comparing measured $\delta^{13}C_{DIC}$ values and DIC concentrations to those expected from conservative mixing, deviations can be defined as:

$$\Delta(\delta^{13}C_{DIC} \times DIC) = \delta^{13}C_{DIC}^{meas} \times DIC^{meas}\text{-}\delta^{13}C_{DIC}^{cons} \times DIC^{cons} \quad (15)$$

During OM degradation, DIC enters the seawater ecosystem with a relatively constant $\delta^{13}C$ value (denoted as $\delta^{13}C_{OM}$), allowing for mass balance expression of isotopic DIC composition:

$$\delta^{13}C_{DIC}^{meas} \times DIC^{meas} = \delta^{13}C_{DIC}^{cons} \times DIC^{cons}+\delta^{13}C_{OM} \times DIC_{OM} \quad (16)$$

where DIC_{OM} and $\delta^{13}C_{OM}$ are the concentration and isotopic composition of DIC released from OC degradation, with DIC_{OM} equal to ΔDIC in equation (7).

Thus, equation (15) can be rearranged into:

$$\Delta(\delta^{13}C_{DIC} \times DIC) = \delta^{13}C_{OM} \times \Delta DIC \quad (17)$$

3. Results

3.1. Sea surface distributions of temperature, salinity, and carbonate parameters in winter

In winter, SST ranged from 18.1 to 18.6 °C, while SSS varied between 23.4 and 28.3 (Fig. 2a and b). Elevated SST (>18.5 °C) with low SSS (<27.3) was observed north of Sandu Island, indicating the influence of river plumes as noted by Han et al. (2024). In contrast, stations along the Dongchong Peninsula had lower SST (18.2–18.5 °C) and SSS (24.2–26.6), reflecting different water mass influences. Additionally, stations south of Sandu Island recorded SST below 18.3 °C and SSS below 24.2, while the central main channel maintained SST around 18.3 °C and SSS near 28.0.

TA and DIC showed similar spatial patterns, ranging from 1975 to 2105 μmol kg^{-1} for TA and from 1890 to 2010 μmol kg^{-1} for DIC (Fig. 2c and d). Higher values (>2080 μmol kg^{-1} for TA; >1980 μmol kg^{-1} for DIC) were founded on the right side of the study area, whereas lower

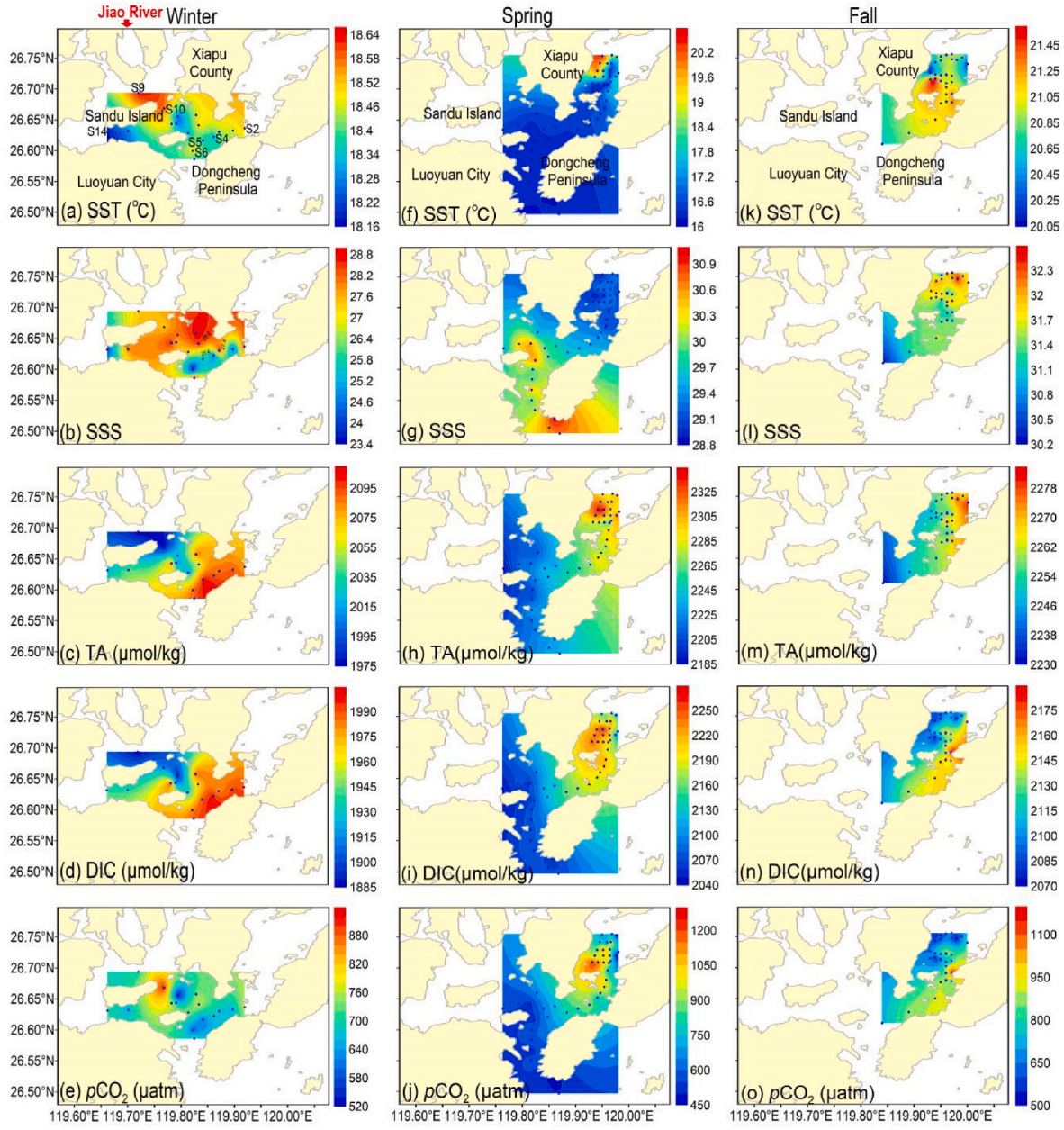

Fig. 2. Spatial distributions of temperature (°C), salinity, dissolved inorganic carbon (DIC, μmol kg^{-1}), total alkalinity (TA, μmol kg^{-1}), and $pCO_{2@in\ situ}$ (μatm) in the surface seawater during the winter cruise in 2021 (a–e), spring cruise in 2024 (f–j), and fall cruise in 2022 (k–o).

values (<2040 μmol kg^{-1} for TA; <1940 μmol kg^{-1} for DIC) extended from the upper-left corner near Sandu Island to the central main channel. Sea surface pCO_2 ranged from 520 to 900 μatm (Fig. 2e), with lower values (<650 μatm) along the Dongchong Peninsula coast.

3.2. Sea surface distributions of temperature, salinity, and carbonate parameters in spring

In spring, SST ranged from 16.0 to 20.3 °C, and SSS varied between 28.8 and 31.1 (Fig. 2f and g). High SST (>19 °C) was noted in Dongwuyang, decreasing towards outer Sansha Bay, while SSS was lowest (<29.4) in Dongwuyang, increasing to 30 in the main channel and reaching up to 31 in outer Sansha Bay. TA and DIC showed similar patterns: TA ranged from 2185 to 2330 μmol kg^{-1} and DIC from 2040 to 2270 μmol kg^{-1} (Fig. 2h and i), both significantly higher in Dongwuyang than the main channel. Surface pCO_2 varied widely from 450 to 1220 μatm (Fig. 2j), with elevated levels (850–1220 μatm) in Dongwuyang compared to lower values (<850 μatm) in the main channel and outer Sansha Bay.

During the cruise, DO ranged from 147 to 240 μmol kg^{-1}; low values (<200 μmol kg^{-1}) were found in Dongwuyang while high values (>220 μmol kg^{-1}) occurred in the main channel. AOU ranged from 0 to 97 μmol kg^{-1}, with higher values recorded in Dongwuyang compared to lower ones observed in the main channel (Fig. 3b). The $\delta^{13}C_{DIC}$ fluctuated between −3.21 ‰ and −0.19 ‰, with averages of −2.50 ‰ in Dongwuyang and −0.75 ‰ in the main channel (Fig. 3c).

3.3. Sea surface distributions of temperature, salinity, and carbonate parameters in fall

In fall, SST ranged from 20.0 to 21.5 °C and SSS from 30.2 to 32.4 (Fig. 2k and l). Both parameters were higher in Dongwuyang compared to the main channel. TA and DIC levels varied between 2230 and 2270 μmol kg^{-1} and 2070–2180 μmol kg^{-1}, respectively, with significantly

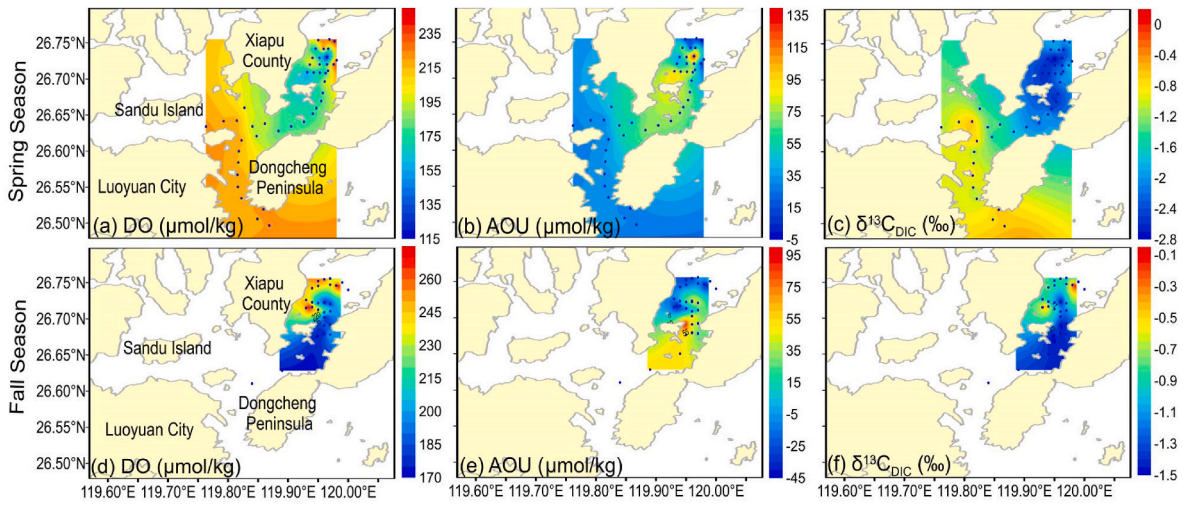

Fig. 3. Surface distributions of dissolved oxygen (DO, μmol kg^{-1}), apparent oxygen utilization (AOU, μmol kg^{-1}), and $\delta^{13}C_{DIC}$ (‰) during the spring cruise in 2024 (panels a–c) and fall cruise in 2022 (panels d–f).

elevated values in Dongwuyang (Fig. 2m and n). Sea surface pCO_2 ranged from 500 to 1150 μatm, consistently higher in Dongwuyang (Fig. 2o). DO, AOU and $\delta^{13}C_{DIC}$ showed ranges of 170~265 μmol kg^{-1}, -25~55 μmol kg^{-1}, and -1.50 ‰~-0.50 ‰, respectively ((Fig. 3d–f).

3.4. Water masses and mixing schemes in Sansha Bay

During winter, carbonate dynamics in Sansha Bay were influenced by two distinct water masses (Fig. 4a). In the main channel, both TA and DIC showed similar distribution patterns with strong linear correlations to salinity (Fig. 4b and c). The relationship was described by TA = 69.9 × Salinity+725 (R^2 = 0.86), with an intercept of ~725 μmol kg^{-1} aligning with coastal river freshwater (RW) end-members (500–1000 μmol kg^{-1}; Qian et al., 2019; Wang et al., 2015), indicating significant influence from coastal plume waters of the Jiao River (Han et al., 2021a, 2024). Along the Dongchong Peninsula coast, a strong linear relationship between surface TA and salinity was also observed (TA = 4.96 × Salinity+1980, R^2 = 0.81), suggesting additional sources of TA beyond freshwater inputs (Akhand et al., 2021; Dai et al., 2021; Jiang et al., 2021; La Valle et al., 2023). Although SBW features were not monitored this season due to limited sampling locations, most winter measurements for TA and DIC fell within the theoretical conservative mixing line between SBW and RW (Fig. 4b and c), reinforcing the influence of both waters masses.

In contrast to the winter cruise focused on the main channel, the spring cruise covered a broader area from outer to inner bay, including Dongwuyang. In the main channel, Sansha Bay Water (SBW) was identified at a salinity of ~30 (Fig. 4b) (Han et al., 2021a). SBW is widespread throughout this region with relatively low SST (<18.5 °C), DIC (<2080 μmol kg^{-1}) and TA (<2250 μmol kg^{-1}) (Fig. 4a–c). In Dongwuyang, a strong linear relationship between TA and salinity was found (TA = −73.5 × Salinity+4500, R^2 = 0.92). This intercept closely matches reported values for SGD end-member concentrations (Table 1, Wang et al., unpublished data), confirming significant SGD influence during spring.

In fall, the water mass composition at Dongwuyang simplified, with TA values primarily aligning with the conservative mixing line of ECSSW and SBW (Fig. 4b), indicating contributions from both water masses. The influence of RW was not detected during spring and fall cruises, likely due to sampling stations being mainly in Dongwuyang,

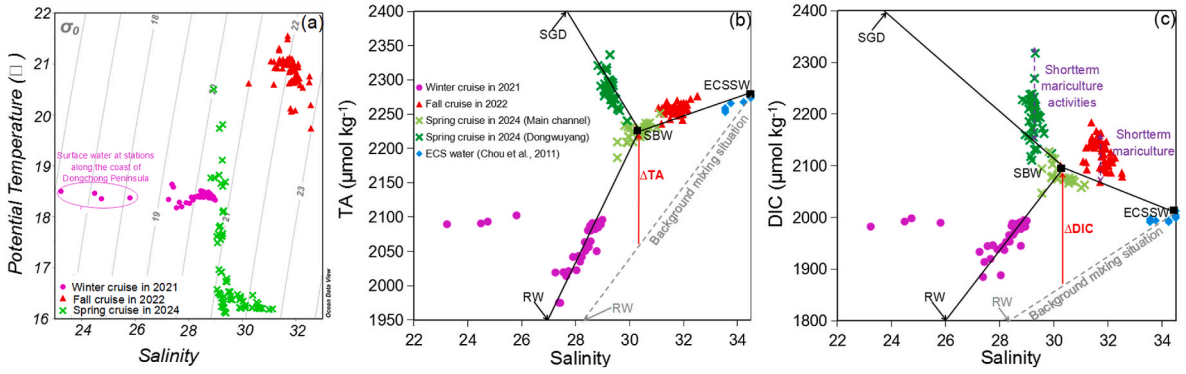

Fig. 4. Relationship between potential temperature and salinity (a), TA and salinity (b), and DIC and salinity (c) in Sansha Bay. Purple dotes, red triangles, and green crosses represent measurements taken during the winter cruise in 2021, fall cruise in 2022, and spring cruise in 2024, respectively. In panels (b) and (c), the end-member of East China Sea (ECS) water was derived from observational data obtained by Chou et al. (2011). Black squares and arrows denote end-members (i.e., Submarine Groundwater Discharge (SGD), River Water (RW), Sansha Bay Water (SBW), East China Sea Surface Water (ECSSW)). The black solid lines represent hypothetical conservative mixing lines between different end members. The gray dashed lines indicate the conservative mixing of RW and ECSSW, representing the background mixing situations in the study area; while the red arrows indicate net TA and DIC additions from long term mariculture activities such as seaweed cultivation, shellfish farming, fish farming, as well as other natural processes like $CaCO_3$ dissolution. Purple arrows in panel c highlight the differences between predicted DIC values and field observations, representing variability caused by short term mariculture activities. (For interpretation of the references to colour in this figure legend, the reader is referred to the Web version of this article.)

Table 1
Summary of end-member values of water mass properties in Sansha Bay. The end-member values for Sansha Bay Water (SBW) were derived from surface measurements collected at stations within the main channel during the fall cruise of 2022. The end-member values for East China Sea Surface Water (ECSSW) represent averaged surface measurements obtained from stations located off the Taiwan Strait, as reported by Chou et al. (2011) and Wang et al. (2016). End-member values for River Water (RW) were sourced from Qian et al. (2019) and Wang et al. (2015), while data on Submarine Groundwater Discharge (SGD) was obtained from Wang et al. (unpublished data) along with measurements conducted by our research group during the spring cruise of 2024 (unpublished data). The composition of DIC stable carbon isotopes ($\delta^{13}C_{DIC}$) for SBW was derived from our measurenemts, while the corresponding values for ECSSW and SGD were obtained from Wang et al. (2016), Dorsett et al. (2011), and Kameyama et al. (2004), respectively. The $pCO_{2@18\ ^\circ C}$ is calculated at the annual average SST.

Situations	End-members	Salinity	TA (μmol kg^{-1})	DIC (μmol kg^{-1})	$pCO_{2@18\ ^\circ C}$ (μatm)	$\delta^{13}C_{DIC}$
Background situation	RW	0	700	700	–	–
	ECSSW	34.50	2279	2013	343	0.60
Driving forces	SBW	30.24	2230	2100	659	−0.87
	SGD	0	4500	4500	–	−18

where freshwater discharge had no significant impact. However, some river water effects may have occurred in the main channel during these seasons.

To summarize, surface water in the main channel during winter is characterized by a two end-member mixing of RW and SBW. In spring, the surface water in Dongwuyang likely resulted from a two end-member mix of SBW and SGD; in fall, it showed a mix of SBW and ECSSW (Fig. 4b and c). As a coastal ecosystem adjacent to the ECS, water proprieties in Sansha Bay are largely influenced by the mixing of ECSSW and RW alongside intensive mariculture activities and natural processes (Bu et al., 2024; Han et al., 2021a, 2024). Thus, we hypothesized that a two end-member mixing model of RW and ECSSW would represent background conditions of Sansha Bay while excluding occasional SGD influences (Fig. 4b and c).

4. Discussion

4.1. A comparison between our observations and other studies on sea surface pCO_2 and air-sea CO_2 flux

In Sansha Bay, sea surface pCO_2 levels ranged from 500 to 1100 μatm in the main channel and Dongwuyang (Fig. 2e, j, and 2o), significantly exceeding the atmospheric level of 440 μatm. Our findings closely align with those of Wei et al. (2016) and Deng et al. (2025), indicating a strong CO_2 source year-round. Following the methodology outlined in section 2.4, we calculated instantaneous air-sea CO_2 fluxes in the main channel at 5.1 ± 1.7 mmol m^{-2} d^{-1} during winter, notably higher than spring of 2.1 ± 1.4 mmol m^{-2} d^{-1}. In Dongwuyang, air-sea CO_2 flux in spring was significantly greater than fall, recorded at 7.0 ± 3.8 mmol m^{-2} d^{-1} compared to 4.7 ± 0.9 mmol m^{-2} d^{-1}.

Generally, natural algal ecosystems, such as seagrass beds (Liu et al., 2024) and areas with natural algal blooms (Xiong et al., 2023), along with macroalgae mariculture systems (Han et al., 2017, 2025; Jiang et al., 2015; Liu et al., 2022; Xiong et al., 2024) primarily function as CO_2 sinks (Table 2). This aligns with the view that seaweed cultivation areas act as carbon sink ecosystems due to their ability to absorb CO_2 through photosynthesis while increasing TA in aquatic environments (Tang et al., 2011). However, the effectiveness of these carbon sinks varies spatially and temporally based on factors like seaweed growth cycles (Li et al., 2021; Liu et al., 2022; Xiong et al., 2023, 2024), seasonal temperature changes (Li et al., 2021; Xiong et al., 2024), and water exchange between coastal regions and open seas (Yang et al., 2025). For example, during vigorous seaweed growth when they mainly act as CO_2 sinks, they may switch to being CO_2 sources at the end of their growth cycle when organic matter decomposes instead (Xiong et al., 2023). Additionally, in marginal ecosystems with significant seasonal SST variations, like those in Sanggou Bay, increases in SST can raise pCO_2 levels from 289 ± 8 μatm to 573 ± 10 μatm between spring and fall. This variation significantly affects seasonal fluctuations of sea surface pCO_2 (Li et al., 2021).

However, in ecosystems where seaweed and shellfish coexist, such as natural coral reefs (Isah et al., 2022) or mariculture areas with mixed cultivation (Han et al., 2017, 2025; Jiang et al., 2015; Liu et al., 2022; Zhou et al., 2024), these systems can act as either CO_2 sinks or sources (Table 2). Their sink-source dynamics show significant spatiotemporal variability, mainly influenced by the carbon utilization of shellfish and seaweed and ongoing mariculture activities (Jiang et al., 2015; Zhou et al., 2024). In contrast, fish farming areas consistently function as CO_2 sources (Table 2) due to inputs from formulated feed (Isah et al., 2022; Liu et al., 2023).

Our findings differ significantly from those observed in other seaweed mariculture regions. It is hypothesized that semi-enclosed mariculture zones with high densities of shellfish and fish farming may greatly influence the carbonate system. Consequently, macroalgal mariculture areas in Sansha Bay are likely to act primarily as a CO_2 source. However, the mechanisms through which various mariculture practices affect the carbonate system remain unclear. Therefore, subsequent sections will focus on clarifying this issue.

4.2. Identifying the factors influencing seasonal dynamics of sea surface pCO_2 in Sansha Bay

In coastal ecosystems, sea surface pCO_2 distributions is mainly influenced by water mass mixing, temperature effects, and biological processes (Zhai et al., 2013; Zhao et al., 2020). To assess their contributions to pCO_2 variability, we analyzed the logarithm of pCO_2 ($\ln pCO_2$) against SST and the temperature-normalized pCO_2 ($npCO_2$) against SSS (Fig. 5). The $npCO_2$ was normalized to 18 °C (annual average SST) following Takahashi et al. (1993) and Wanninkhof et al. (2022).

In winter, a logarithmic relationship between $\ln pCO_2$ and SST was observed across all main channel stations ($\ln pCO_2 = 0.43 \times SST\text{-}1.28$, $R^2 = 0.28$, Fig. 5a). The slope exceeds the typical ratio of $\partial \ln pCO_2/\partial T = 0.0423\ ^\circ C^{-1}$ reported by Takahashi et al. (2009), indicating that temperature has minimal influence on pCO_2 distributions within this narrow range (<0.5 °C). In contrast, a strong linear relationship between $npCO_2$ and salinity was founded ($npCO_2 = 20.86 \times SSS + 138.97$, $R^2 = 0.53$, Fig. 5b), underscoring the significant role of water mass mixing in regulating spatial variability.

In spring, distinct patterns for $\ln pCO_2$ and $npCO_2$ emerged between the main channel and Dongwuyang with no significant correlation between $\ln pCO_2$ and SST in either area (Fig. 5c). This suggests that while temperature affects pCO_2 levels, it does not fully explain spatial variations. In the main channel, lower $npCO_2$ values indicate that a two end-member mixing process primarily governs variability; however, Dongwuyang showed no significant correlation between $npCO_2$ and SSS (Fig. 5d), suggesting limited mixing influence on its variability.

In fall, the relationship between surface $\ln pCO_2$ and SST in Dongwuyang is described by $\ln pCO_2 = 0.05 \times SST + 5.62$ ($R^2 = 0.33$) (Fig. 5e), highlighting the significant impact of temperature on pCO_2 dynamics. A positive correlation between $npCO_2$ and SSS was also observed ($npCO_2 = 149.64 \times SSS + 40.50$, $R^2 = 0.46$, Fig. 5f), indicating that water mass mixing plays a crucial role in shaping pCO_2 distribution patterns.

Using end-member values from Table 1, we predicted pCO_2 through conservative mixing of different end-members (Fig. 5b, d, 5f). A two

Table 2
A systematic review of sea surface pCO_2 and air-sea CO_2 flux in mariculture ecosystems along the Chinese mainland coast and globally. It is important to note that studies derived from laboratory experiments, mass balance model calculations, or measurements conducted in mariculture ponds and coastal high-density aquaculture facilities have been excluded from this review.

Domains	Types	Mariculture activities	Months/Seasons	Sinks/ Sources	pCO_2 (μatm)	Air-sea CO_2 flux (mmol/m^2/d)	Reference
Other countries	Coral reefs in Philippines	Fish Farming	May during dry seasons	CO_2 source	953 ± 35	–	Isah et al. (2022)
		Nearest natural coral reef ecosystem		CO_2 source	512 ± 15	–	
		Medium distance natural coral reef ecosystem		CO_2 source	514 ± 49	–	
		Farthest natural coral reef ecosystem		CO_2 source	492 ± 47	–	
		Offshore		CO_2 source	477 ± 28	–	
		Total		CO_2 source	552 ± 153	–	
		Fish Farming	August and September during the wet seasons	CO_2 source	483 ± 25	–	
		Nearest natural coral reef ecosystem		CO_2 source	525 ± 109	–	
		Medium distance natural coral reef ecosystem		CO_2 sink	406 ± 22	–	
		Farthest natural coral reef ecosystem		CO_2 source	464 ± 25	–	
		Offshore		CO_2 sink	398 ± 3	–	
		Total		CO_2 source	459 ± 72	–	
	A shellfish farming bay in Korea	Shellfish farming	January in Winter	CO_2 sink	263.28	−14.03	Shim et al. (2021)
			February in Winter	CO_2 sink	247.79	−15.19	
			March in Spring	CO_2 sink	249.89	−13.42	
			April in Spring	CO_2 sink	282.54	−10.72	
			May in Spring	CO_2 sink	335.31	−3.5	
			June in Summer	CO_2 sink	396.33	−0.34	
			July in Summer	CO_2 source	448.78	1.5	
			August in Summer	CO_2 source	474.92	2.66	
			September in Fall	CO_2 source	464.86	2.81	
			October in Fall	CO_2 source	422.67	1.04	
			November in Fall	CO_2 sink	363.68	−2.57	
			December in Winter	CO_2 sink	305.88	−9.46	
Domain 1: Coastal mariculture ecosystems in the Yellow sea, Bohai Sea, and Northern Yellow Sea	A shellfish farming bay near Yangma Island	Shellfish farming	March in Spring	CO_2 sink	353.6 ± 98.2	−3.32 ± 6.13	Yang et al. (2021b)
			May in Spring	CO_2 source	~600	5.74 ± 8.79	
			June in Summer	CO_2 source	460.7 ± 21.8	2.31 ± 5.26	
			July in Summer	CO_2 source	~750	16.32 ± 8.72	
			August in Summer	CO_2 source	~650	13.06 ± 9.26	
			September in Fall	CO_2 source	850.8 ± 285.6	25.77 ± 16.30	
			November in Fall	CO_2 source	~450	4.49 ± 1.81	
	A mariculture ecosystem in Sanggou Bay	Seaweed farming	April in Spring	CO_2 sink	~300–400	~-35	Liu et al. (2022)
			July in Summer	CO_2 sink	~340–440	~-20	
			October in Fall	CO_2 sink	~300–360	~-45	
			January in Winter	CO_2 sink	~300–340	~-60	
		Shellfish and Seaweed farming	April in Spring	CO_2 sink	~300–400	~-25	
			July in Summer	CO_2 source	~340–440	~2.5	
			October in Fall	CO_2 sink	~300–360	~-40	
			January in Winter	CO_2 sink	~300–340	~-48	
		Shellfish farming	April in Spring	CO_2 sink	~300–400	~-5	
			July in Summer	CO_2 source	~340–440	~5	
			October in Fall	CO_2 sink	~300–360	~-25	
			January in Winter	CO_2 sink	~300–340	~-35	
		Shellfish farming	May in Spring	CO_2 sink	~240	–	Qiu et al. (2013)

(continued on next page)

Table 2 (*continued*)

Domains	Types	Mariculture activities	Months/Seasons	Sinks/ Sources	pCO_2 (μatm)	Air-sea CO_2 flux (mmol/m^2/d)	Reference
		Shellfish and Seaweed farming		CO_2 sink	310~320	–	
		Shellfish	May in Spring	CO_2 sink	350~360	–	Liu et al. (2017)
		Shellfish and Seaweed		CO_2 sink	~350	–	
		Seaweed		CO_2 sink	320~350	–	
		Shellfish	August in Summer	CO_2 sink	~360	–	
		Shellfish and Seaweed		CO_2 sink	345~360	–	
		Seaweed		CO_2 sink	340~360	–	
		Seaweed farming	May in Spring	CO_2 sink	289 ± 8	−28.56 ± 5.77	Li et al. (2021)
			June in Summer	CO_2 sink	370 ± 4	−5.10 ± 6.70	
			July in Summer	CO_2 source	405 ± 4	0.45 ± 3.25	
			August in Summer	CO_2 source	452 ± 9	4.73 ± 3.66	
			September in Fall	CO_2 source	573 ± 1	16.71 ± 2.08	
		Shellfish farming	May in Spring	CO_2 source	446 ± 2	8.90 ± 3.47	
			June in Summer	CO_2 source	505 ± 3	13.47 ± 2.71	
			July in Summer	CO_2 source	527 ± 6	10.92 ± 1.56	
			August in Summer	CO_2 source	516 ± 6	8.77 ± 4.49	
			September in Fall	CO_2 source	783 ± 8	36.06 ± 6.78	
		Seaweed farming	April in Spring	CO_2 sink	~210	–	Zhang et al. (2013)
			August in Summer	CO_2 sink	~220	–	
			October in Fall	CO_2 source	~380	–	
			January in Winter	CO_2 sink	~295	–	
		Shellfish and Seaweed farming	April in Spring	CO_2 sink	~220	–	
			August in Summer	CO_2 sink	~240	–	
			October in Fall	CO_2 sink	~320	–	
			January in Winter	CO_2 sink	~270	–	
		Shellfish zone	April in Spring	CO_2 sink	~280	–	
			August in Summer	CO_2 sink	~80	–	
			October in Fall	CO_2 sink	~300	–	
			January in Winter	CO_2 sink	~220	–	
		Shellfish farming and seaweed farming,	April in Spring	CO_2 sink	–	−109.21 ± 21.42	Jiang et al. (2015)
			June in Summer	CO_2 source	–	125.43	
			October in Fall	CO_2 source	–	30~46.8	
			January in Winter	CO_2 sink	–	−115.9~-132.37	
		Shellfish farming -Newly built	July in Summer	CO_2 source	755 ± 20	–	Li et al. (2024)
		Shellfish farming -Long standing	July in Summer	CO_2 sink	755 ± 14	–	
		Seaweed farming	April in Spring	CO_2 sink	~250	–	Han et al. (2025)
			June in Summer	CO_2 sink	~360	–	
			October in Fall	CO_2 sink	~250	–	
			January in Winter	CO_2 sink	~320	–	
		Shellfish and Seaweed farming	April in Spring	CO_2 sink	~320	–	
			June in Summer	CO_2 source	~410	–	
			October in Fall	CO_2 sink	~240	–	
			January in Winter	CO_2 sink	~310	–	
		Shellfish farming	April in Spring	CO_2 sink	~350	–	
			June in Summer	CO_2 source	~420	–	
			October in Fall	CO_2 sink	~220	–	
			January in Winter	CO_2 sink	~290	–	
		Seaweed farming	September in Fall	CO_2 source	~550	–	Xiong et al. (2024)
			November in Fall	CO_2 sink	~418	–	
			January in Winter	CO_2 sink	~300	–	
			March in Spring	CO_2 sink	~295	–	
			May in Spring	CO_2 sink	~290	–	
			June in Summer	CO_2 sink	~418	–	
			July in Summer	CO_2 sink	~418	–	
			August in Summer	CO_2 source	~450	–	
	A seaweed mariculture area in Lidao Bay	Seaweed farming	April in Spring	CO_2 sink	267.7 ± 31.6	~-49.00	Jiang et al. (2013)

(*continued on next page*)

Table 2 (*continued*)

Domains	Types	Mariculture activities	Months/Seasons	Sinks/ Sources	pCO_2 (μatm)	Air-sea CO_2 flux (mmol/m^2/d)	Reference
			August in Summer	CO_2 sink	328.3 ± 20.9	~-14.00	
			October in Fall	CO_2 sink	264.7 ± 13.1	~-38.00	
			January in Winter	CO_2 sink	285.2 ± 16.3	~-45.00	
		Seaweed farming	June in Summer	CO_2 sink	325.78 ± 0.15	–	Xiao et al. (2021)
	A natural macroalgal bloom area in Qingdao	Before Macroalgal Blooms	March in Spring 2018)	CO_2 sink	397 ± 45	–	Xiong et al. (2023)
		Late Macroalgal Blooms	July in Summer 2018)	CO_2 source	541 ± 60	–	
		After Macroalgal Blooms	October in Fall 2018)	CO_2 source	528 ± 80	–	
		Before Macroalgal Blooms	March in Spring 2019)	CO_2 source	400 ± 41	–	
		Late Macroalgal Blooms	July in Summer 2019)	CO_2 source	617 ± 61	–	
		After Macroalgal Blooms	October in Fall 2019)	CO_2 source	674 ± 208	–	
	A macroalgae-shellfish mariculture area in Haizhou Bay	Shellfish farming and Seaweed farming	July in Summer	CO_2 sink	349.16 ± 114.9	−4.5	Zhou et al. (2024)
			November in Fall	CO_2 sink	243.68 ± 74.41	−24.10	
			January in Winter	CO_2 sink	161.99 ± 104.34	−37.68	
			March in Spring	CO_2 sink	180.92 ± 67.48	−38.99	
Domain 2: Coastal mariculture ecosystems in the Chhangjiang River Estuary and adjacent coastal areas	A shellfish mariculture area of Gouqi Island	Shellfish farming	July in Summer	CO_2 source	–	13.09 ± 3.19	He et al. (2024)
		Shellfish farming	October in Fall	CO_2 source	–	41.40 ± 5.23	
		Shellfish farming	May in Spring	CO_2 sink	–	−0.15 ± 0.07	
	A shellfish mariculture area of Gouqi Island	Shellfish farming	July in Summer	CO_2 sink	402 ± 58.1	−2.232 ± 10.19	Chang et al. (2022)
		Shellfish farming	October in Fall	CO_2 sink	411 ± 98.52	−0.476 ± 19.62	
		Shellfish farming	January in Winter	CO_2 source	677 ± 15.36	85.91 ± 4.95	
		Shellfish farming	May in Spring	CO_2 sink	320.9 ± 83.62	−16.91 ± 15.27	
	A mariculture ecosystem in Xiangshan Bay	Shellfish farming	January in Winter	CO_2 sink	367 ± 83	−1.8 ± 2.6	Yang et al. (2025)
			April in Spring	CO_2 source	639 ± 52	2.7 ± 0.6	
			July in Summer	CO_2 source	527 ± 36	1.5 ± 0.5	
			October in Fall	CO_2 source	491 ± 36	2.4 ± 1.1	
Domain 3: Coastal mariculture ecosystems in the coastal regions of Fujian Province	A mariculture ecosystem in Sansha Bay	Shellfish farming, seaweed farming, and fish farming	November in Fall	CO_2 source	724.66 ± 58.41	3.37 ± 0.48	Wei et al. (2016)
			February in Winter	CO_2 source	572.99 ± 32.63	2.30 ± 0.72	
			May in Spring	CO_2 source	744.44 ± 62.56	3.12 ± 1.85	
			August in Summer	CO_2 source	561.89 ± 28.37	1.29 ± 0.68	
			Annual average	CO_2 source	–	13.44748858	Deng et al. (2025)
	A seaweed mariculture area of Fodu Island	Seaweed farming	November in Fall	CO_2 source	447.37 ± 0.26	–	Xiao et al. (2021)
Domain 4: Coastal mariculture ecosystems in the Pearl River Estuary and adjacent coastal areas	A mariculture ecosystem in Daya Bay	Shellfish farming and fish farming	Annual average	CO_2 sink	–	−19.8 ± 914.6	Han et al. (2016)
		Seaweed farming	April in Spring	CO_2 sink	–	−33.6 ± 4.0	Han et al. (2017)
		Shellfish farming and seaweed farming	April in Spring	CO_2 sink	–	−8.4 ± 0.7	
	A shellfish mariculture area in Kaozhou Bay	Shellfish farming	Summer	CO_2 source	–	42.04 ± 9.56	Peng et al. (2022)
			Fall	CO_2 source	–	276.14 ± 52.55	
			Winter	CO_2 sink	–	−11.59 ± 18.15	
			Spring	CO_2 sink	–	−13.02 ± 6.71	
	A seaweed mariculture area of Nan'ao Island	Seaweed farming	May in Spring	CO_2 sink	270.66 ± 0.54	–	Xiao et al. (2021)
	A mariculture ecosystem in Shenao Bay	Shellfish farming, seaweed farming, and fish farming	February in Winter	CO_2 sink	270 ± 51	–	Wang et al. (2017)
			March in Spring	CO_2 source	416 ± 66	–	

(*continued on next page*)

Table 2 (*continued*)

Domains	Types	Mariculture activities	Months/Seasons	Sinks/ Sources	pCO_2 (μatm)	Air-sea CO_2 flux (mmol/m^2/d)	Reference
			April in Spring	CO_2 sink	100 ± 18	–	
			May in Spring	CO_2 source	399 ± 68	–	
			July in Summer	CO_2 sink	300 ± 67	–	
		Fish farming	March in Spring	CO_2 sink	309.2	−1.2	Han et al. (2021b)
			April in Spring	CO_2 sink	~100	−3.2	
			May in Spring	CO_2 sink	~200	−2	
		Shellfish farming	March in Spring	CO_2 sink	~250	−1.8	
			April in Spring	CO_2 sink	~80	−3.8	
			May in Spring	CO_2 sink	~150	−2.5	
		Seaweed farming	March in Spring	CO_2 sink	56.2	−2.5	
			April in Spring	CO_2 sink	~60	−4.8	
			May in Spring	CO_2 sink	~100	−3.8	
Domain 5: Coastal mariculture ecosystems in Hainan Island	A mariculture ecosystem in Qinglan Bay	Fish farming	July in Summer	CO_2 source	~484–782	9.49 ± 3.69	Liu et al. (2023)
	Natural seagrass meadows of Hainan Island	Natural seagrass meadows in Tanmen	Annual average	CO_2 sink	416	−2.13 ± 0.44	Liu et al. (2024)
		Natural seagrass meadows in Li'an	Annual average	CO_2 sink	364	−1.72 ± 0.36	
		Natural seagrass meadows in Xincun	Annual average	CO_2 sink	365	−1.37 ± 0.30	

end-member model involving RW and ECSSW represents background mixing conditions without mariculture influences (gray dashed lines). In contrast, the conservative mixing of RW, SBW, ECSSW, and SGD reflects annual averaged water properties in Sansha Bay (black solid lines). Discrepancies between these scenarios illustrate changes in pCO_2 due to long-term mariculture activities (red arrows), while differences between predicted values and field observations indicate seasonal variability from short-term activities (purple arrows).

Under background mixing conditions, predicted pCO_2 values ranged from 250 to 350 μatm, lower than atmospheric pCO_2 levels (Fig. 5b, d, 5f). However, long-term mariculture activities increased DIC and TA in SBW (Fig. 4b and c), leading to pCO_2 values of ~660 μatm (Table 1 and Fig. 5d). In the two end-member mixing model, elevated pCO_2 in the SBW end-member significantly raised surface npCO_2 levels in Sansha Bay to between 500 and 700 μatm (Fig. 5b, d, 5f). Consequently, high pCO_2 levels in the SBW end-member dominated CO_2 outgassing processes. Additionally, occasional SGD disturbances could raise pCO_2 by ~30–60 μatm (Fig. 5d), while short-term mariculture activities further affected pCO_2 distributions, causing deviations from conservative mixing lines (Fig. 5b, d, 5f). Thus, the CO_2 source in Sansha Bay was likely influenced by DIC accumulations from long-term mariculture activities and the seasonal DIC cycles related to aquaculture practices. This will be discussed and quantified in sections 4.3 and 4.4.

4.3. Quantifying the long-term carbon dynamics mediated by different mariculture activities in SBW

In Sansha Bay, Lin et al. (2017) simulated hydrodynamics and water exchange processes, revealing that Baima Harbor has a low seawater exchange rate with a half-exchange time exceeding 40 days due to its distance from the bay mouth and weak ebb currents lacking distinct outward flows. Similarly, the eastern head of Dongwuyang also shows a half-exchange time over 40 days, likely caused by weak tidal and inward residual currents. As a result, continuous net release of DIC and TA during mariculture activities throughout the year, combined with prolonged half-exchange times, may lead to their accumulation in bay water. This causes significantly higher concentrations of these parameters in the SBW end-member compared to background conditions (indicated by red arrows in Fig. 4b and c). Utilizing end-member values from Table 1, we estimated the additions of DIC and TA (ΔDIC and ΔTA) at 229 ± 19 μmol kg^{-1} and 137 ± 11 μmol kg^{-1}, respectively. Following methodologies outlined in texts S1 and S2, we first assessed carbon removal and sequestration across various mariculture ecosystems before apportioning these DIC and TA additions among different activities while simulating pCO_2 dynamics influenced by these processes.

4.3.1. Background situation

In Sansha Bay, the estimated DIC and TA values from the conservative mixing of ECSSW and RW were 1845 ± 14 μmol kg^{-1} and 2077 ± 16 μmol kg^{-1} for SBW, indicating a background scenario with relatively low DIC and TA. Additionally, natural $CaCO_3$ dissolution increases seawater DIC and TA by 108 ± 8 μmol kg^{-1} and 216 ± 17 μmol kg^{-1}, respectively. Similar effects have been observed in various coastal ecosystems such as the Pearl River Estuary (PRE) (Guo et al., 2020), Sanya Bay coral reefs (Wang et al., 2014), and Yellow Sea shellfish mariculture areas (Yang et al., 2021b).

During our cruises, Ω_{arag} at all stations exceeded 1.5 (data not shown), suggesting that in situ $CaCO_3$ dissolution was unlikely in Sansha Bay (Ekstrom et al., 2015; Gruber et al., 2012; Li and Zhai, 2019; Waldbusser et al., 2015). Instead, natural $CaCO_3$ dissolution here likely reflects long-term weathering processes over hundreds of years within the surrounding drainage basin (Yang et al., 2021a). This weathering transports DIC and TA to Sansha Bay via river systems. The higher TA intercepts ranging from 725 to 1980 μmol kg^{-1} from river discharges support this influence. Furthermore, elevated DIC and TA concentrations of up to 4500 μmol kg^{-1} found in SGD can be partially attributed to $CaCO_3$ dissolution due to weathering processes (Dai et al., 2021; Yang et al., 2022). SGD contributes further to the accumulation of DIC and TA within Sansha Bay.

Consequently, we estimate that the DIC and TA values attributable to natural processes (mixing and $CaCO_3$ dissolution) are 1953 ± 9 μmol kg^{-1} and 2293 ± 11 μmol kg^{-1}, respectively (Fig. 6a). The calculated natural background pCO_2 is therefore determined to be 199 ± 7 μatm, indicating a strong CO_2 sink for the SBW (Fig. 6a and b).

4.3.2. Seaweed cultivation

In Sansha Bay, seaweed photosynthesis in spring and winter is vital for absorbing atmospheric CO_2. However, the decomposition of residual biomass after harvest releases CO_2 into seawater during summer and fall (Wei et al., 2016). With a reported seaweed production of 30 × 10^4 tons, it sequesters 4.32 × 10^4 tons of carbon annually as DIC while releasing 1.31 × 10^4 tons back into seawater. This results in a net removal of 3.01 × 10^4 tons of carbon per year. In SBW, seaweed cultivation decreases DIC by 46 ± 4 μmol kg^{-1} and increase TA by 7 ± 1 μmol kg^{-1} (Fig. 6a).

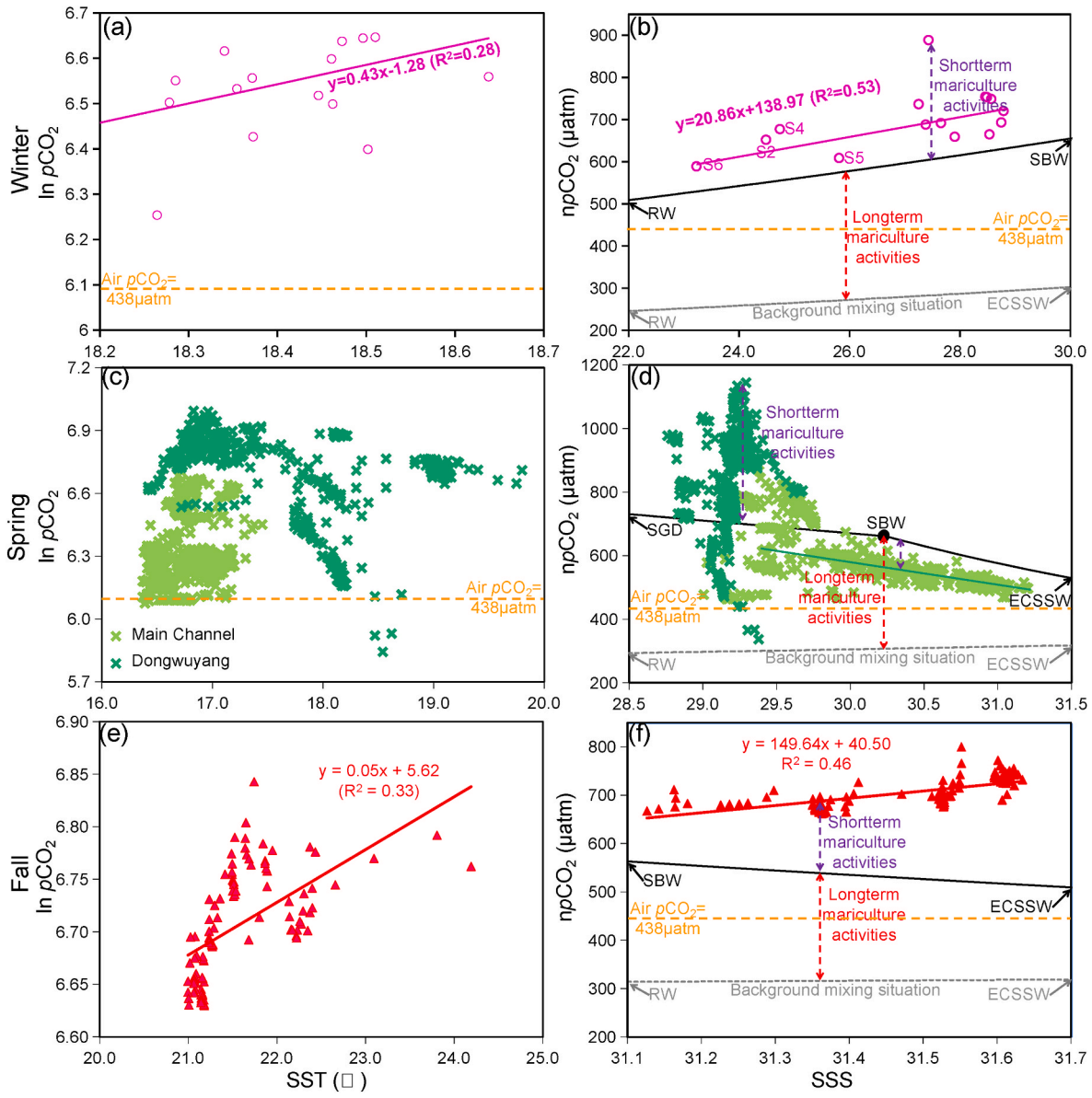

Fig. 5. Relationships between pCO_2 (logarithmic) and sea surface temperature (SST, left column) and temperature-normalized pCO_2 ($npCO_2$) and sea surface salinity (SSS, right column) during the winter cruise in 2021 (a, b), the spring cruise in 2024 (c and d), and the fall cruise in 2022 (e and f). The pink and red solid lines in panels a and e represent the linear relationships between $lnpCO_2$ and SST, while the green and red solid lines in panels b, d and f depict the linear relationships between $npCO_2$ and SSS. In panels b, d, f, the gray dashed lines indicate the conservative mixing of RW and ECSSW, which represents the background mixing conditions in the study area. Additionally, the red arrows illustrate the long term pCO_2 increase from mariculture activities. Purple arrows in panels b, d, and f highlight the differences between predicted pCO_2 values and field observations, representing seasonal variability caused by short term mariculture activities. In all panels, yellow dashed lines represent the air pCO_2 of 438 µatm. (For interpretation of the references to colour in this figure legend, the reader is referred to the Web version of this article.)

Consequently, this practice reduces sea surface pCO_2 by ~42 ± 5 µatm (Fig. 6a and b), enhancing CO_2 uptake in mariculture areas. This reduction indicates significant potential for achieving carbon neutrality through seaweed cultivation (Fig. 6b).

4.3.3. Shellfish farming

In shellfish farming, the carbon sequestered from shell harvests is estimated at 1.78×10^4 tons carbon per year. In contrast, the growth of shellfish and organic material respiration release 1.85×10^4 tons of carbon annually into seawater. Thus, shellfish farming results in a net increase of 7.0×10^2 tons of carbon each year. While it has a negligible effect on DIC concentrations, it significantly reduces TA by an average of 55 ± 5 µmol kg^{-1} (Fig. 6a). This reduction in TA raises seawater pCO_2 by ~36 ± 4 µatm, counteracting reductions linked to seaweed cultivation (Fig. 6b).

4.3.4. Fish farming

Fish product harvesting removes carbon at a rate of 3.84×10^4 tons per year; however, formulated feed contributes an estimated input of 1.92×10^5 tons annually. Consequently, fish farming leads to a net release of 1.075×10^5 tons of carbon into seawater each year. This process causes DIC levels in seawater to rise significantly by 166 ± 14 µmol kg^{-1} while decreasing TA by 27 ± 3 µmol kg^{-1} (Fig. 6a). As a result, fish farming increases seawater pCO_2 notably by ~375 ± 18 µatm to unprecedented levels around ~567 ± 20 µatm (Fig. 6b), transforming this mariculture area from a strong CO_2 sink into a significant source.

The findings indicate that within SBW, DIC generated from fish farming exceeds its consumption during seaweed cultivation and thus

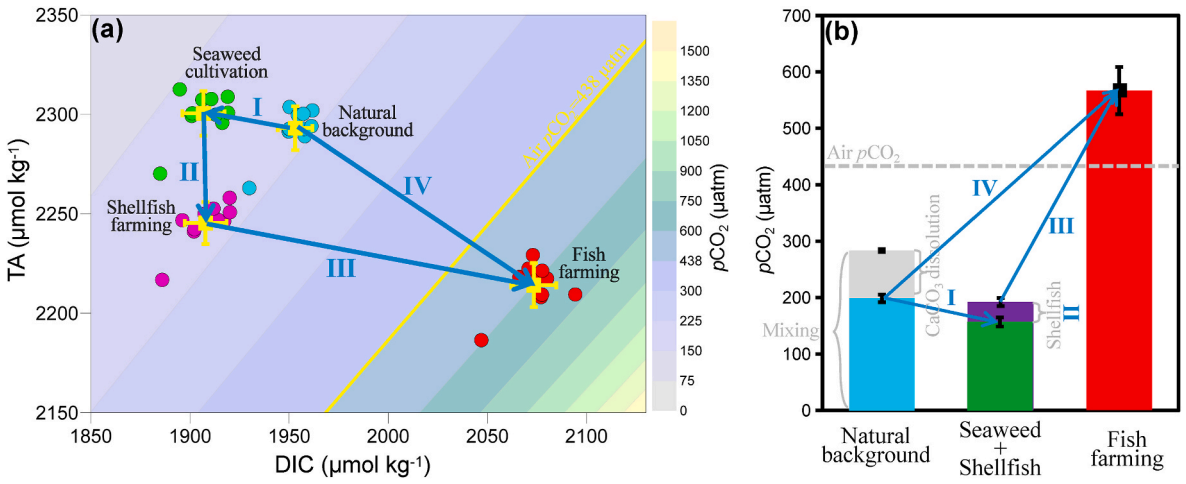

Fig. 6. A simulation of carbon dynamics and surface pCO_2 controlling factors in Sansha Bay Water. In (a), the sky blue circles represent the natural background DIC and TA values simulated from mixing and natural $CaCO_3$ dissolution. The green and purple circles depict the simulated results considering seaweed cultivation and shellfish farming, while the red circles indicate the observed DIC and TA concentrations during the cruise with additional influence from fish farming. The squares and error bars represent average values and standard deviations of SBW. The transition from the natural background situation to the observed situation involves three main steps (b). Step I indicates DIC consumption during seaweed growth, step II indicates a moderate decrease in TA during shellfish farming, and step III denotes DIC increase during fish farming due to decomposition of organic matter from formulated feed. Step IV represent the net influence of anthropogenic mariculture activities on the dynamics of DIC, TA and pCO_2. Please note that all simulations and analysis were conducted based on the DIC and TA of water samples collected from the main channel during the spring cruise in 2024. (For interpretation of the references to colour in this figure legend, the reader is referred to the Web version of this article.)

dominates the overall increase in DIC. Although shellfish growth typically consumes TA through $CaCO_3$ formation, this is balanced out by natural $CaCO_3$ weathering in the surrounding drainage basin leading to an overall increase in TA. The elevated levels of DIC and TA create conditions with high pCO_2 values that sustain CO_2 outgassing at the sea surface in Sansha Bay.

4.4. Tracing the short-term dynamics of DIC mediated by different mariculture activities in Sansha Bay

Although SGD raises sea surface pCO_2 levels in Dongwuyang during spring (Fig. 5d), short-term pCO_2 dynamics are mainly driven by mariculture activities across all three seasons (Fig. 5b, d and 5f). The respiration of organic materials from these activities increases seasonal DIC

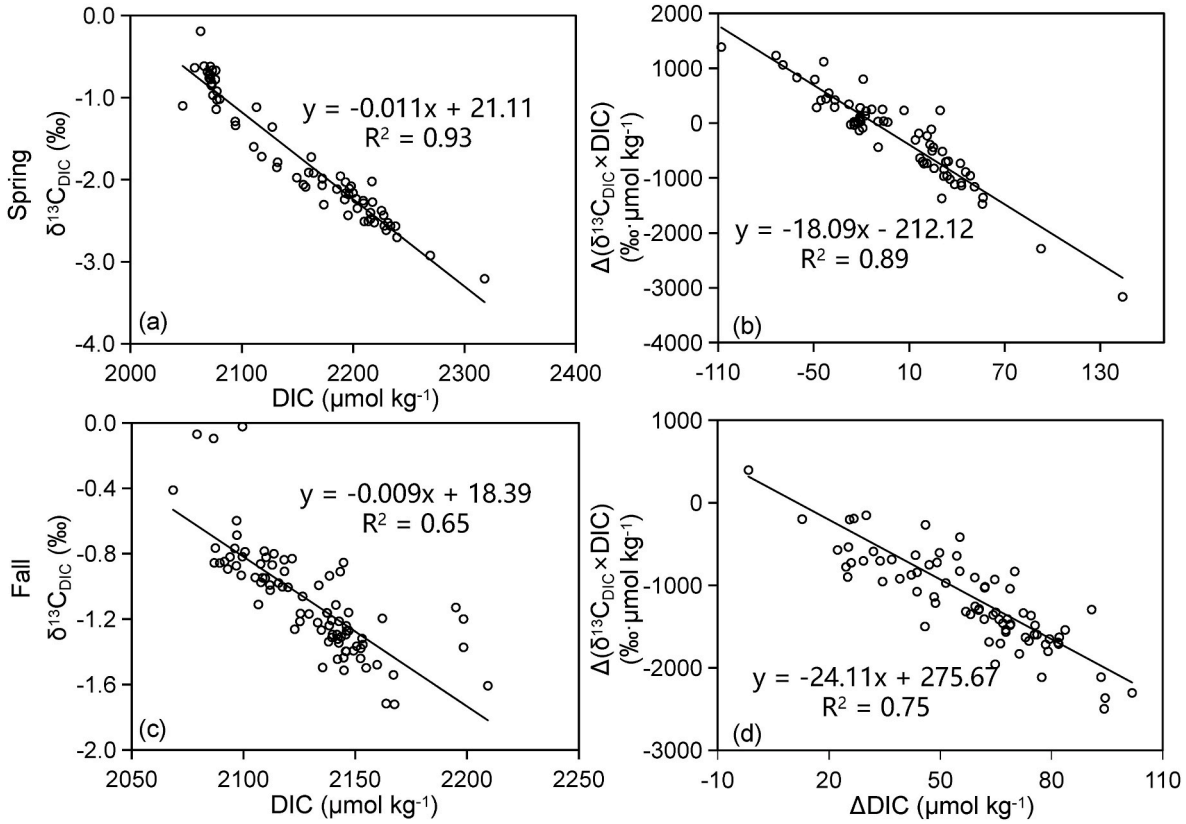

Fig. 7. Linear relationships of $\delta^{13}C_{DIC}$-DIC and $\Delta(\delta^{13}C_{DIC} \times DIC)$-ΔDIC during the spring cruise in 2024 (panels a and b) and fall cruise in 2022 (panels c and d).

concentrations, elevating seawater pCO_2 to ~1100 μatm and enhancing CO_2 outgassing in Sansha Bay. This section investigates the sources of oxygen-consuming organic matter in Sansha Bay during spring and fall using a semi-analytical diagnostic method based on $\delta^{13}C_{DIC}$.

In spring, high AOU values were noted with lower $\delta^{13}C_{DIC}$ distributions in Dongwuyang, while the main channel and outer bay showed low AOU but high $\delta^{13}C_{DIC}$ values (Fig. 3b and c). The negative correlation between AOU and $\delta^{13}C_{DIC}$ (Fig. 7a) indicates that metabolic processes significantly affect DIC dynamics (Wang et al., 2016; Zhao et al., 2020). However, the measured ratio of DIC to AOU was found to be 1.84, diverging from the classic Redfield ratio of ~0.77 (Chen et al., 2022; Dong et al., 2017; Redfield et al., 1963), likely due to O_2 replenishment from air-sea exchange (Chen et al., 2022; Ouyang et al., 2024).

During the cruise, a strong negative correlation was observed between $\Delta(\delta^{13}C_{DIC} \times DIC)$ and ΔDIC (Fig. 7b), with a slope of −18.09 ‰ indicating the original $\delta^{13}C$ signature of remineralized organic matter. The isotopic composition closely resembles of marine sourced POC, ranging from −22.0 ‰ to −18 ‰ (Chen et al., 2022; Su et al., 2017; Wang et al., 2016; Zhang et al., 2025; Zhao et al., 2020). This suggests that oxygen-consuming organic matter in spring at Sansha Bay is predominantly derived from marine sources, accounting for nearly 100 %. Furthermore, these $\delta^{13}C$ signatures align with those of particulate organic matter from in situ phytoplankton production in Sansha Bay (~16.94 ‰; Han et al., 2024), indicating that decomposition of residual seaweed biomass during late spring significantly contributes to increases in DIC.

In fall, both AOU and $\delta^{13}C_{DIC}$ exhibited mirrored distribution patterns (Fig. 3e and f). Similar to spring, the negative relationship between AOU and $\delta^{13}C_{DIC}$ (Fig. 7c) further supports metabolic processes regulating DIC dynamics. Additionally, the ratio of DIC to AOU was found to be 0.89, aligning closely with the Redfield ratio and providing strong evidence for aerobic respiration of organic carbon (Chen et al., 2022; Dong et al., 2017; Redfield et al., 1963).

The $\delta^{13}C$ values of fall water samples were more isotopically depleted (−24.11 ‰; Fig. 7d) than those obtained in spring (~18.09 ‰), indicating different organic carbon sources. These $\delta^{13}C$ signatures range between marine and terrestrial POC, specifically −22.0 ‰ to −18 ‰ for marine and −32 ‰ to −25 ‰ for terrestrial sources (Chen et al., 2022; Su et al., 2017; Wang et al., 2016; Zhang et al., 2025; Zhao et al., 2020). This suggests that oxygen-consuming organic matter in Sansha Bay during fall comes from both marine and terrestrial origins. Previous studies show that the $\delta^{13}C$ value in fish feed is ~ -23.4 ‰ (Han et al., 2024), aligning with our findings. Thus, we conclude that the seasonal increase in DIC during fall results from the respiration of organic matter derived from formulated fish feed.

4.5. Methods for achieving carbon neutrality in Sansha Bay

Fish farming has a significantly different impact than seaweed cultivation and shellfish farming, leading to an increase in seawater DIC (Fig. 6a). This is mainly due to the respiration of formulated feed that settles in sediment during fish farming, which offsets CO_2 uptake from photosynthesis during seaweed growth. In Sansha Bay, garbage fish used as feed contributes over 86–90 % of the total anthropogenic carbon and nutrients load (Han et al., 2024; Ji et al., 2021). Studies indicate that this formulated feed greatly adds to organic loading in the marine environment, resulting in increased DIC and enhanced CO_2 outgassing at the surface (Isah et al., 2022; Ji et al., 2021; Lin et al., 2019; Liu et al., 2023; Yang et al., 2021c).

To fully sequester carbon released from fish farming in Sansha Bay, seaweed cultivation would need to expand fourfold without changes in productivity. However, findings by Gao et al. (2022b), Guan et al. (2022), and Zhang et al. (2022) show that China's key cultivated seaweeds only increased their area and annual productivity by 20–30 % between 2010 and 2020 at both national level and specifically for Fujian Province. If this rate continues, achieving carbon neutrality solely through expanding seaweed cultivation area is impractical due to limited space in Sansha Bay.

To achieve carbon neutrality in Sansha Bay, it is recommended to reduce fish farming production or area by 80 %. However, farmed aquatic products accounts for 25 % of China's national animal protein consumption (Xie et al., 2022), meaning that a reduction in fish production could significantly impact food security. To tackle this issue, exploring a farming model that maximizes material efficiency is essential. Integrated multi-trophic aquaculture (IMTA) has gained attention over the past decade due to its ecological efficiency and environmental safety (Fang et al., 2020; Liu et al., 2022; Xie et al., 2022). This approach involves co-cultivating various aquaculture species at different trophic levels within a shared environment, including fed species (like fish), inorganic extractors (such as seaweeds), and organic extractors (filter-feeding and deposit-feeding organisms) (Qiu et al., 2013).

From a carbon cycling perspective, IMTA enhances carbon utilization while reducing dependence on external inputs like formulated feed. Consequently, CO_2 emissions from the aquaculture ecosystem can be effectively reduced (Liu et al., 2022; Troell et al., 2009). Research indicates that in IMTA systems, whether in eutrophic bays or open environments, seaweeds can effectively utilize nutrients from fish farming wastewater for growth while absorbing DIC (Chopin et al., 2004, 2013; Lander et al., 2004; Qiu et al., 2013; Troell and Norberg, 1998; Troell et al., 2009). Shellfish growth is influenced by suspended matter concentration around them; their filtration can reduce suspended particulate matter by over 50 %, inhibiting carbon mineralization and release (Lander et al., 2004; Neori et al., 2017; Troell and Norberg, 1998). Observational data suggest that the IMTA model could lower sea surface pCO_2 levels by up to 70 μatm. In certain seasons, an IMTA system may even act as a CO_2 sink (Liu et al., 2022; Qiu et al., 2013). Thus, implementing IMTA may be crucial for achieving carbon neutrality goals in Sansha Bay.

5. Conclusion

This study examined the carbonate system in Sansha Bay, China's largest macroalgae mariculture area. Our result reveled that it acts as a strong CO_2 source during winter, spring, and fall, contrary to the expectation that macroalgae mariculture areas are CO_2 sinks due to carbon burial in sediments. Quantitative analysis shows that in this semi-enclosed bay, DIC produced from fish farming surpasses its consumption during seaweed cultivation, leading to an overall increase in DIC and pCO_2. Intensive fish farming has transformed Sansha Bay from a strong CO_2 sink into a source, greatly reducing the region's carbon sequestration capacity. Additionally, seasonal SGD and short-term mariculture activities may further elevate pCO_2 and enhance CO_2 outgassing at the sea surface. To achieve mCDR and protect coastal environments, it is essential to reduce formulated feed use or develop alternative environmentally friendly fish farming methods like IMTA.

CRediT authorship contribution statement

Wei Yang: Writing – review & editing, Writing – original draft, Methodology, Investigation, Formal analysis. **Yingxu Wu:** Validation, Investigation, Writing – review & editing. **Yanmei Liu:** Investigation, Formal analysis. **Peiqiang Zhuang:** Investigation. **Chenglong Li:** Validation, Methodology, Investigation. **Jianhang Zhang:** Methodology, Investigation. **Yingfeng Chen:** Methodology, Investigation. **Yanpei Zhuang:** Methodology, Formal analysis. **Hongyang Lin:** Methodology. **Huaji Qiu:** Methodology. **Youjun Huang:** Methodology. **Weijie Qiu:** Methodology. **Wei-Jun Cai:** Writing – review & editing. **Liqi Chen:** Validation, Formal analysis. **Di Qi:** Writing – review & editing, Validation, Supervision, Methodology, Investigation, Funding acquisition, Formal analysis.

Declaration of competing interest

None declared.

Acknowledgement

This work received support from the Ocean Negative Carbon Emissions (ONCE) Program. This work is also supported by National Key Research and Development Program of China (2023YFC3108102), the Science Foundation of Fujian Province, China (Grant No. 2023J01797, 2024J01114), the Science Foundation of Xiamen, Fujian Province (Grant No. 3502Z20227051), the Science Foundation of Fujian Educational Bureau (Grant No. JAT220178), and the Major Undergraduate Teaching Reform Project in Fujian Province (Grant No. FBJY20230123).

Appendix A. Supplementary data

Supplementary data to this article can be found online at https://doi.org/10.1016/j.marenvres.2025.107515.

Data availability

Data will be made available on request.

References

Akhand, A., Watanabe, K., Chanda, A., Tokoro, T., Chakraborty, K., Moki, H., et al., 2021. Lateral carbon fluxes and CO_2 evasion from a subtropical mangrove-seagrass-coral continuum. Sci. Total Environ. 752, 142190.

Benson, B.B., Krause Jr., D., 1984. The concentration and isotopic fractionation of oxygen dissolved in freshwater and seawater in equilibrium with the atmosphere 1. Limnol. Oceanogr. 29 (3), 620–632.

Bu, D., Zhu, Q., Li, J., Huang, J., Zhuang, Y., Yang, W., Qi, D., 2024. Mariculture may intensify eutrophication but lower N/P ratios: a case study based on nutrients and dual nitrate isotope measurements in Sansha Bay, southeastern China. Front. Mar. Sci. 11, 1351657.

Cai, W.J., Jiao, N., 2022. Wastewater alkalinity addition as a novel approach for ocean negative carbon emissions. Innovation 3 (4).

Cai, W.J., Dai, M., Wang, Y., Zhai, W., Huang, T., Chen, S., et al., 2004. The biogeochemistry of inorganic carbon and nutrients in the Pearl River estuary and the adjacent Northern South China Sea. Cont. Shelf Res. 24 (12), 1301–1319.

Chang, J., Duan, Y., Zhang, J., Shen, Y., Shen, Q., Zhao, S., et al., 2022. Carbon flux and carbon sequestration capacity in a shellfish culture area of Gouqi Island. J. Fish. Sci. China 29, 1589–1600 (in Chinese).

Chen, Z.Y., Zhai, W.D., Yang, S., Zhang, Y., Liu, P.F., 2022. Exploring origin of oxygen-consuming organic matter in a newly developed quasi-hypoxic coastal ocean, the Bohai Sea (China): a stable carbon isotope perspective. Sci. Total Environ. 837, 155847.

Chopin, T., Robinson, S., Sawhney, M., Bastarache, S., Belyea, E., Shea, R., 2004. The AquaNet integrated multi-trophic aquaculture project: rationale of the project and development of kelp cultivation as the inorganic extractive component of the system. Bull. Aquacult. Assoc. Can. 104, 11–18.

Chopin, T., Robinson, S., Reid, G., Ridler, N., 2013. Prospects for Integrated Multi-Trophic Aquaculture (IMTA) in the open ocean. Bull. Aquacult. Assoc. Can. 111, 28–35.

Chou, W.C., Gong, G.C., Tseng, C.M., Sheu, D.D., Hung, C.C., Chang, L.P., Wang, L.W., 2011. The carbonate system in the East China Sea in winter. Mar. Chem. 123 (1–4), 44–55.

Clawson, G., Kuempel, C.D., Frazier, M., Blasco, G., Cottrell, R.S., Froehlich, H.E., et al., 2022. Mapping the spatial distribution of global mariculture production. Aquaculture 553, 738066.

Dai, G., Wang, G., Li, Q., Tan, E., Dai, M., 2021. Submarine groundwater discharge on the western shelf of the northern South China Sea influenced by the Pearl River plume and upwelling. J. Geophys. Res.: Oceans 126 (4), e2020JC016859.

Deng, Y., Guo, X., Zhao, X., Zhou, H., Li, L., Chen, Y., Zhu, X., 2025. Coastal macroalgae aquaculture reduces carbon dioxide emission in a subtropical enclosed bay: insights from eddy covariance measurements. Agric. Ecosyst. Environ. 385, 109576.

Dickson, A.G., 1990. Standard potential of the reaction: $AgCl(s)+12H_2(g)=Ag(s)+HCl(aq)$, and and the standard acidity constant of the ion HSO_4^- in synthetic sea water from 273.15 to 318.15 K. J. Chem. Therm. 22 (2), 113–127.

Dong, X., Huang, H., Zheng, N., Pan, A., Wang, S., Huo, C., et al., 2017. Acidification mediated by a river plume and coastal upwelling on a fringing reef at the east coast of H ainan I sland, N orthern S outh C hina S ea. J. Geophys. Res.: Oceans 122 (9), 7521–7536.

Dorsett, A., Cherrier, J., Martin, J., Cable, J., 2011. Assessing hydrologic and biogeochemical controls on pore-water dissolved inorganic carbon cycling in a subterranean estuary: a ^{14}C and ^{13}C mass balance approach. Mar. Chem. 127 (1), 76–89.

Ekstrom, J.A., Suatoni, L., Cooley, S.R., Pendleton, L.H., Waldbusser, G.G., Cinner, J.E., et al., 2015. Vulnerability and adaptation of US shellfisheries to ocean acidification. Nat. Clim. Change 5 (3), 207–214.

Fang, J., Fang, J., Chen, Q., Mao, Y., Jiang, Z., Du, M., et al., 2020. Assessing the effects of oyster/kelp weight ratio on water column properties: an experimental IMTA study at Sanggou Bay, China. J. Oceanol. Limnol. 38 (6), 1914–1924.

Friedlingstein, P., Jones, M.W., O'Sullivan, M., Andrew, R.M., Bakker, D.C., Hauck, J., et al., 2022. Global carbon budget 2021. Earth Syst. Sci. Data 14 (4), 1917–2005.

Froehlich, H.E., Afflerbach, J.C., Frazier, M., Halpern, B.S., 2019. Blue growth potential to mitigate climate change through seaweed offsetting. Curr. Biol. 29 (18), 3087–3093.

Gao, G., Beardall, J., Jin, P., Gao, L., Xie, S., Gao, K., 2022a. A review of existing and potential blue carbon contributions to climate change mitigation in the Anthropocene. J. Appl. Ecol. 59 (7), 1686–1699.

Gao, G., Gao, L., Jiang, M., Jian, A., He, L., 2022b. The potential of seaweed cultivation to achieve carbon neutrality and mitigate deoxygenation and eutrophication. Environ. Res. Lett. 17 (1), 014018.

Gruber, N., Hauri, C., Lachkar, Z., Loher, D., Frölicher, T.L., Plattner, G.K., 2012. Rapid progression of ocean acidification in the California Current system. science 337 (6091), 220–223.

Guo, X., Song, X., Gao, Y., Luo, Y., Xu, Y., Huang, T., Wang, L., 2020. Inter-annual variability of the carbonate system in the hypoxic upper pearl River Estuary in winter. Front. Mar. Sci. 7, 594725.

Guan, H., Sun, Z., Zhao, A., 2022. Spatio-temporal evolution and influencing factors of net carbon sink in marine aquaculture in China. Front. Environ. Sci. 10, 978073.

Han, A.Q., Dai, M.H., Gan, J.P., Kao, S.J., Zhao, X.Z., Jan, S., et al., 2013. Inter-shelf nutrient transport from the East China Sea as a major nutrient source supporting winter primary production on the northeast South China Sea shelf. Biogeosciences 10 (12), 8159–8170.

Han, T., Qi, Z., Wu, F., Liao, X., Ma, S., Fu, G., Huang, H., 2016. Comparative study of dissolved inorganic carbon systems of surface waters in various oceanic functional areas of Daya Bay. J. Tropical Oceanogr. 35, 57–65 (in Chinese).

Han, T., Shi, R., Qi, Z., Huang, H., Liang, Q., Liu, H., 2017. Interactive effects of oyster and seaweed on seawater dissolved inorganic carbon systems: implications for integrated multi-trophic aquaculture. Aquac. Environ. Interact. 9, 469–478.

Han, A., Kao, S.J., Lin, W., Lin, Q., Han, L., Zou, W., et al., 2021a. Nutrient budget and biogeochemical dynamics in Sansha Bay, China: a coastal bay affected by intensive mariculture. J. Geophys. Res.: Biogeosciences 126 (9), e2020JG006220.

Han, T., Shi, R., Qi, Z., Huang, H., Gong, X., 2021b. Impacts of large-scale aquaculture activities on the seawater carbonate system and air-sea CO_2 flux in a subtropical mariculture bay, southern China. Aquac. Environ. Interact. 13, 199–210.

Han, A., Yang, J.Y.T., Chen, M., Zheng, Z., Yin, X., Lin, H., et al., 2024. Hydrological connectivity controls on the dynamics of particulate organic matter in a semi-enclosed mariculture bay. Aquaculture 578, 740109.

Han, T., Shi, R., Qi, Z., Liu, Q., Huang, H., 2025. Role of intensive mariculture on CO_2 absorption and carbon burial, and the carbon sink potential of Sanggou Bay, China. Aquaculture 597, 741936.

He, J., Tao, Y., Shao, S., Wei, H., Yan, G., Tang, C., et al., 2024. The hidden acceleration pump uncovers the role of shellfish in oceanic carbon sequestration. Sci. Total Environ. 951, 175699.

Isah, R.R., Enochs, I.C., San Diego-McGlone, M.L., 2022. Sea surface carbonate dynamics at reefs of Bolinao, Philippines: seasonal variation and fish mariculture-induced forcing. Front. Mar. Sci. 9, 858853.

Ji, W., Yokoyama, H., Fu, J., Zhou, J., 2021. Effects of intensive fish farming on sediments of a temperate bay characterised by polyculture and strong currents. Aquaculture Rep. 19, 100579.

Jiang, Z., Fang, J., Han, T., Li, J., Mao, Z., Wang, W., 2013. Estimation of sea-air CO_2 flux in seaweed aquaculture area. Lidao Bay Progres Fishery Sci. 34, 50–56 (in Chinese).

Jiang, Z., Li, J., Qiao, X., Wang, G., Bian, D., Jiang, X., et al., 2015. The budget of dissolved inorganic carbon in the shellfish and seaweed integrated mariculture area of Sanggou Bay, Shandong, China. Aquaculture 446, 167–174.

Jiang, Z.P., Lv, J., Li, Q., Dai, M., Kao, S.J., Zheng, N., Fan, W., 2021. Tidal-driven submarine groundwater discharge and its influences on the carbonate system of a coastal coral reef in the Northern South China Sea. J. Geophys. Res.: Oceans 126 (7), e2021JC017203.

Jiao, N., Wang, H., Xu, G., Aricò, S., 2018. Blue carbon on the rise: challenges and opportunities. Natl. Sci. Rev. 5 (4), 464–468.

Jiao, N.Z., Liu, J.H., Shi, T., Zhang, C., Zhang, Y., Zheng, Q., et al., 2021. Deploying ocean negative carbon emissions to implement the carbon neutrality strategy. Scientia Sinica Terrae 51 (4), 632–643 (in Chinese).

La Valle, F.F., Jacobs, J.M., Thomas, F.I., Nelson, C.E., 2023. Nutrient-rich submarine groundwater discharge increases algal carbon uptake in a tropical reef ecosystem. Front. Mar. Sci. 10, 1178550.

Lander, T., Barrington, K., Robinson, S., MacDonald, B., Martin, J., 2004. Dynamics of the blue mussel as an extractive organism in an integrated multi-trophic aquaculture system. Bull. Aquacult. Assoc. Can. 104, 19–28.

Lee, K., Kim, T.W., Byrne, R.H., Millero, F.J., Feely, R.A., Liu, Y.M., 2010. The universal ratio of boron to chlorinity for the North Pacific and North Atlantic oceans. Geochem. Cosmochim. Acta 74 (6), 1801–1811.

Li, C.L., Zhai, W.D., 2019. Decomposing monthly declines in subsurface-water pH and aragonite saturation state from spring to autumn in the North Yellow Sea. Cont. Shelf Res. 185, 37–50.

Li, J., Zhang, W., Ding, J., Xue, S., Huo, E., Ma, Z., et al., 2021. Effect of large-scale kelp and bivalve farming on seawater carbonate system variations in the semi-enclosed Sanggou Bay. Sci. Total Environ. 753, 142065.

Li, J., Jiang, Z., Zhang, M., Sun, X., Jiao, M., Li, J., et al., 2024. Large-scale oyster farming accelerates the removal of dissolved inorganic carbon from seawater in Sanggou Bay. Mar. Environ. Res. 202, 106798.
Li, W., Zhang, S., Lu, C., 2022. Exploration of China's net CO_2 emissions evolutionary pathways by 2060 in the context of carbon neutrality. Sci. Total Environ. 831, 154909.
Liu, Y., Lin, F., Wu, W., Wu, N., Zhang, Y., Wang, W., Li, M., Zhang, J., 2017. Seasonal variations (spring and summer) of the surface seawater pCO_2 in Sanggou Bay and corresponding impact factors. J. Fish. Sci. China 24, 1107–1114 (in Chinese).
Liu, Y., Zhang, J., Wu, W., Zhong, Y., Li, H., Wang, X., et al., 2022. Effects of shellfish and macro-algae IMTA in north China on the environment, inorganic carbon system, organic carbon system, and sea-air CO_2 fluxes. Front. Mar. Sci. 9, 864306.
Liu, J., Chen, Y., Wang, Y., Du, M., Wu, Z., 2023. Greenhouse gases emissions and dissolved carbon export affected by submarine groundwater discharge in a maricultural bay, Hainan Island, China. Sci. Total Environ. 857, 159665.
Liu, S., Liang, J., Jiang, Z., Li, J., Wu, Y., Fang, Y., et al., 2024. Temporal and spatial variations of air-sea CO_2 fluxes and their key influence factors in seagrass meadows of Hainan Island, South China Sea. Sci. Total Environ. 910, 168684.
Lin, H., Chen, Z., Hu, J., Cucco, A., Zhu, J., Sun, Z., Huang, L., 2017. Numerical simulation of the hydrodynamics and water exchange in Sansha Bay. Ocean. Eng. 139, 85–94.
Lin, H., Chen, Z., Hu, J., Cucco, A., Sun, Z., Chen, X., Huang, L., 2019. Impact of cage aquaculture on water exchange in Sansha Bay. Cont. Shelf Res. 188, 103963.
Lueker, T.J., Dickson, A.G., Keeling, C.D., 2000. Ocean pCO_2 calculated from dissolved inorganic carbon, alkalinity, and equations for K1 and K2: validation based on laboratory measurements of CO_2 in gas and seawater at equilibrium. Mar. Chem. 70 (1–3), 105–119.
Mathis, M., Lacroix, F., Hagemann, S., Nielsen, D.M., Ilyina, T., Schrum, C., 2024. Enhanced CO_2 uptake of the coastal ocean is dominated by biological carbon fixation. Nat. Clim. Change 14 (4), 373–379.
Neori, A., Shpige, M., Guttman, L., Israel, A., 2017. Development of polyculture and integrated multi-trophic aquaculture (IMTA) in Israel: a review. Isr. J. Aquac. Bamidgeh 69.
Nguyen, P.Q., 2024. Groundwater quality assessment in the middle-upper Pleistocene aquifer. Civl Eng. J. 10 (7), 2357–2369.
Ouyang, Z., Fujiwara, A., Nishino, S., Murata, A., Li, Q., Hatta, M., et al., 2024. Source partitioning of dissolved inorganic carbon addition to Pacific Winter Water in the western Arctic Ocean. Limnol. Oceanogr. 69 (11), 2532–2546.
Oyinlola, M.A., Reygondeau, G., Wabnitz, C.C., Troell, M., Cheung, W.W., 2018. Global estimation of areas with suitable environmental conditions for mariculture species. PLoS One 13 (1), e0191086.
Peng, P., Ma, Y., Shi, R., Wang, D., Xu, X., Yan, B., 2022. Temporal and spatial variation in the sea-air CO_2 flux in the oyster aquaculture area of Kaozhou Bay. Mar. Sci. 46, 140–149 (in Chinese).
Qian, W., Chen, Y., Yang, L.M., Peng, Y.Z., Zhang, L., Li, T.Y., Jiang, M.H., 2019. Carbon fractions and fluxes in the lower reach of Minjiang River. Res. Environ. Sci. 32, 647–653 (in Chinese).
Qiu, S., Gong, B., Zhang, J., Ren, L., Liu, Z., Zhang, L., 2013. Distribution and affecting factors of pCO_2 in aquaculture areas of Sanggou Bay during spring. Progress Fishery Sci. 34, 31–37 (in Chinese).
Redfield, A.C., Ketchum, B.H., Richards, F.A., 1963. The influence of organisms on the composition of seawater. Sea 2 (2), 26–77.
Salt, L.A., Beaumont, L., Blain, S., Bucciarelli, E., Grossteffan, E., Guillot, A., et al., 2016. The annual and seasonal variability of the carbonate system in the Bay of Brest (Northwest Atlantic Shelf, 2008-2014). Mar. Chem. 187, 1–15.
Salter, I., Schiebel, R., Ziveri, P., Movellan, A., Lampitt, R., Wolff, G.A., 2014. Carbonate counter pump stimulated by natural iron fertilization in the Polar Frontal Zone. Nat. Geosci. 7 (12), 885–889.
Shim, J., Ye, M.J., Lim, J.H., Kwon, J.N., Kim, J.B., 2021. Red tide events and seasonal variations in the partial pressure of CO_2 and related parameters in shellfish-farming bays, Southeastern coast of Korea. Front. Mar. Sci. 8, 738472.
Su, J., Dai, M., He, B., Wang, L., Gan, J., Guo, X., et al., 2017. Tracing the origin of the oxygen-consuming organic matter in the hypoxic zone in a large eutrophic estuary: the lower reach of the Pearl River Estuary, China. Biogeosciences 14 (18), 4085–4099.
Takahashi, T., Olafsson, J., Goddard, J.G., Chipman, D.W., Sutherland, S.C., 1993. Seasonal variation of CO_2 and nutrients in the high-latitude surface oceans: a comparative study. Glob. Biogeochem. Cycles 7 (4), 843–878.
Takahashi, T., Sutherland, S.C., Wanninkhof, R., Sweeney, C., Feely, R.A., Chipman, D. W., et al., 2009. Climatological mean and decadal change in surface ocean pCO2, and net sea-air CO_2 flux over the global oceans. Deep Sea Res. Part II Top. Stud. Oceanogr. 56 (8–10), 554–577.
Tang, Q., Zhang, J., Fang, J., 2011. Shellfish and seaweed mariculture increase atmospheric CO_2 absorption by coastal ecosystems. Mar. Ecol. Prog. Ser. 424, 97–104.
Tang, J., Ye, S., Chen, X., Yang, H., Sun, X., Wang, F., et al., 2018. Coastal blue carbon: concept, study method, and the application to ecological restoration. Sci. China Earth Sci. 61, 637–646.
Troell, M., Norberg, J., 1998. Modelling output and retention of suspended solids in an integrated salmon-mussel culture. Ecol. Model. 110, 65–77.
Troell, M., Joyce, A., Chopin, T., Neori, A., Buschmann, A.H., Fang, J.G., 2009. Ecological engineering in aquaculture-potential for integrated multi-trophic aquaculture (IMTA) in marine offshore systems. Aquaculture 297, 1–9.
Troell, M., Henriksson, P.J., Buschmann, A.H., Chopin, T., Quahe, S., 2022. Farming the ocean–seaweeds as a quick fix for the climate? Rev. Fish. Sci. Aquac. 31 (3), 285–295.
van Heuven, S., Pierrot, D., Rae, J.W.B., Lewis, E., Wallace, D.W.R., 2011. MATLAB program developed for CO_2 system calculations. Oak Ridge, Tennessee: Carbon Dioxide Information Analysis Center. Oak Ridge National Laboratory, U.S. Department of Energy.
Waldbusser, G.G., Hales, B., Langdon, C.J., Haley, B.A., Schrader, P., Brunner, E.L., et al., 2015. Saturation-state sensitivity of marine bivalve larvae to ocean acidification. Nat. Clim. Change 5 (3), 273–280.
Wanninkhof, R., 2014. Relationship between wind speed and gas exchange over the ocean revisited. Limnol Oceanogr. Methods 12 (6), 351–362.
Wanninkhof, R., Pierrot, D., Sullivan, K., Mears, P., Barbero, L., 2022. Comparison of discrete and underway CO_2 measurements: inferences on the temperature dependence of the fugacity of CO_2 in seawater. Mar. Chem. 247, 104178.
Wang, G., Jing, W., Wang, S., Xu, Y., Wang, Z., Zhang, Z., et al., 2014. Coastal acidification induced by tidal-driven submarine groundwater discharge in a coastal coral reef system. Environ. Sci. Technol. 48 (22), 13069–13075.
Wang, G., Wang, Z., Zhai, W., Moore, W.S., Li, Q., Yan, X., et al., 2015. Net subterranean estuarine export fluxes of dissolved inorganic C, N, P, Si, and total alkalinity into the Jiulong River estuary, China. Geochem. Cosmochim. Acta 149, 103–114.
Wang, H., Dai, M., Liu, J., Kao, S.J., Zhang, C., Cai, W.J., et al., 2016. Eutrophication-driven hypoxia in the East China Sea off the changjiang Estuary. Environ. Sci. Technol. 50 (5), 2255–2263.
Wang, J., Du, H., Zhang, Q., Chen, Y., Mei, Z., Chen, W., 2017. The influence of the cultivation of *Gracilaria lemaneiformis* on the pCO_2 in surface waters of Shenao Bay. Ecolo. Sci. 36, 152–159 (in Chinese).
Wang, G., Han, A., Chen, L., Tan, E., Lin, H., 2018. Fluxes of dissolved organic carbon and nutrients via submarine groundwater discharge into subtropical Sansha Bay, China. Estuar. Coast Shelf Sci. 207, 269–282.
Wang, F., Harindintwali, J.D., Yuan, Z., Wang, M., Wang, F., Li, S., et al., 2021. Technologies and perspectives for achieving carbon neutrality. Innovation 2 (4).
Wang, Y., Yang, W., Zhao, X., Zhang, Q., Chen, H., Fang, Z., Zheng, M., 2023a. Changes in the carbon source and storage in a cultivation area of macro-algae in Southeast China. Mar. Pollut. Bull. 188, 114680.
Wang, Y., Yang, W., Cai, Y., Fang, Z., Zhao, X., Zhang, Q., et al., 2023b. Macroalgae culture-induced carbon sink in a large cultivation area of China. Environ. Sci. Pollut. Control Ser. 30 (49), 107693–107702.
Wang, Y., Guo, X., Wang, G., Wang, L., Huang, T., Li, Y., et al., 2024. Assessment of nutrient cycling in an intensive mariculture system. Mar. Pollut. Bull. 209, 117085.
Weitzman, J., Steeves, L., Bradford, J., Filgueira, R., 2019. Far-Field and near-field Effects of Marine Aquaculture. World seas: An environmental evaluation, pp. 197–220.
Wei, Z., Hna, H., Hu, M., Wu, H., Zhang, J., Huo, Y., He, P., 2016. Seasonal variation of sea-air CO_2 flux in mariculture area in Yantian Harbor, Sansha Bay. J. Shanghai Ocean Univ. 25, 106–115 (in Chinese).
Weiss, R., 1974. Carbon dioxide in water and seawater: the solubility of a non-ideal gas. Mar. Chem. 2 (3), 203–215.
Xiao, X., Agustí, S., Yu, Y., Huang, Y., Chen, W., Hu, J., et al., 2021. Seaweed farms provide refugia from ocean acidification. Sci. Total Environ. 776, 145192.
Xiong, T., Li, H., Yue, Y., Hu, Y., Zhai, W., Xue, L., Jiao, N., Zhang, Y., 2023. Legacy effects of late macroalgal blooms on dissolved inorganic carbon pool through alkalinity enhancement in coastal Ocean. ES T (Environ. Sci. Technol.) 57, 2186–2196.
Xiong, T., Li, H., Hu, Y., Zhai, W.D., Zhang, Z., Liu, Y., et al., 2024. Seaweed farming environments do not always function as CO_2 sink under synergistic influence of macroalgae and microorganisms. Agric. Ecosyst. Environ. 361, 108824.
Xie, B., Zhou, X., Huang, L., Zheng, X., Du, J., Yu, W., et al., 2022. The ecological functions and risks of expansive bivalve-macroalgae polyculture: a case study in Sansha Bay, China. Aquaculture 560, 738549.
Yang, W., Guo, X., Cao, Z., Xu, Y., Wang, L., Guo, L., et al., 2021a. Seasonal dynamics of the carbonate system under complex circulation schemes on a large continental shelf: the northern South China Sea. Prog. Oceanogr. 197, 102630.
Yang, B., Gao, X., Zhao, J., Liu, Y., Lui, H.K., Huang, T.H., et al., 2021b. Massive shellfish farming might accelerate coastal acidification: a case study on carbonate system dynamics in a bay scallop (Argopecten irradians) farming area, North Yellow Sea. Sci. Total Environ. 798, 149214.
Yang, B., Gao, X., Zhao, J., Liu, Y., Xie, L., Lv, X., Xing, Q., 2021c. Summer deoxygenation in a bay scallop (Argopecten irradians) farming area: the decisive role of water temperature, stratification and beyond. Mar. Pollut. Bull. 173, 113092.
Yang, W., Guo, X., Cao, Z., Su, J., Guo, L., Wang, L., et al., 2022. Carbonate dynamics in a tropical coastal system in the South China Sea featuring upwelling, river plumes and submarine groundwater discharge. Sci. China Earth Sci. 65 (12), 2267–2284.
Yang, Z., Yang, X., Zhang, C., Jin, Y., Hu, X., Zhou, X., et al., 2025. Seasonal variability of sea surface pCO_2 and air-sea CO_2 flux in a high turbidity coastal ocean in the vicinity of the East China Sea. Front. Mar. Sci. 12, 1580318.
Zhang, Y., Zhang, J., Liang, Y., Li, H., Li, G., Chen, X., et al., 2017. Carbon sequestration processes and mechanisms in coastal mariculture environments in China. Sci. China Earth Sci. 60, 2097–2107.
Zhang, M., Yan, J., Ye, W., Zhang, C., Gao, Z., Xu, C., 2022. Carbon sequestration and its potentiality of marine shellfish and seaweed cultures in Fujian Province, China. J. Appl. Oceanography 41, 53–58 (in Chinese).
Zhang, M., Yang, W., Zhang, J., Lu, C., Wu, Y., Zhuang, P., et al., 2025. Evaluating the impacts of drilling and extraction activities on the marine carbonate system in the natural gas fields of Beibu Gulf, Northern South China Sea. Mar. Environ. Res. 207, 107058.
Zhai, W., Dai, M., Cai, W.J., Wang, Y., Wang, Z., 2005. High partial pressure of CO_2 and its maintaining mechanism in a subtropical estuary: the Pearl River estuary, China. Mar. Chem. 93 (1), 21–32.

Zhai, W.D., Dai, M.H., Chen, B.S., Guo, X.H., Li, Q., Shang, S.L., et al., 2013. Seasonal variations of sea-air CO_2 fluxes in the largest tropical marginal sea (South China Sea) based on multiple-year underway measurements. Biogeosciences 10 (11), 7775–7791.

Zhao, Y., Liu, J., Uthaipan, K., Song, X., Xu, Y., He, B., et al., 2020. Dynamics of inorganic carbon and pH in a large subtropical continental shelf system: interaction between eutrophication, hypoxia, and ocean acidification. Limnol. Oceanogr. 65 (6), 1359–1379.

Zhou, J.H., Guo, Y.Z., Zhao, X., Yu, J.C., Zhou, J., Lin, J., Huang, H., 2024. Impacts of shellfish and macroalgae mariculture on the seawater carbonate system and air-sea CO_2 flux in Haizhou Bay, China. Mar. Environ. Res. 202, 106774.

Zhang, J., Wu, W., Ren, L., Han, T., Wang, W., Fang, J., 2013. Seasonal variation of pCO_2 and its potential influencing factors in aquaculture areas of Sanggou Bay. Progress Fishery Sci. 34, 57–64 (in Chinese).